

Genons, Double Covers and Fault-tolerant Clifford Gates

Simon Burton, Elijah Durso-Sabina, Natalie C. Brown

Quantinuum

June 17, 2024

Abstract

A great deal of work has been done developing quantum codes with varying overhead and connectivity constraints. However, given the such an abundance of codes, there is a surprising shortage of fault-tolerant logical gates supported therein. We define a construction, such that given an input $[[n, k, d]]$ code, yields a $[[2n, 2k, \geq d]]$ *symplectic double* code with naturally occurring fault-tolerant logical Clifford gates. As applied to 2-dimensional $D(\mathbb{Z}_2)$ -topological codes with *genons* (twists) and domain walls, we find the symplectic double is genon free, and of possibly higher genus. Braiding of genons on the original code becomes Dehn twists on the symplectic double. Such topological operations are particularly suited for architectures with all-to-all connectivity, and we demonstrate this experimentally on Quantinuum’s H1-1 trapped-ion quantum computer.

Contents

1	Introduction	2
1.1	Outline	3
1.2	Related work	5
2	Background	6
2.1	$D(\mathbb{Z}_2)$ topological order	6
2.1.1	Example in genus zero	8
2.1.2	Dehn twists	10
2.1.3	Riemann surfaces and double covers	12
2.2	ZX -calculus survival guide	14
2.3	Quantum codes and symplectic geometry	16
2.3.1	The qubit Clifford and Pauli groups	17
3	The symplectic double	19
3.1	Lifting Cliffords	22
4	Genon codes	23
4.1	Genon graphs and genon codes	23
4.2	String operators	25
4.3	Domain walls	28
4.4	Double covers of genon codes	29

5	Example genon codes and protocols	30
5.1	Genus zero	30
5.2	Genus one	32
6	Experimental results	36
6.1	The $[[4,1,2]]$ protocol	37
6.2	The $[[8,2,2]]$ protocol	38
6.3	The $[[10,2,3]]$ protocol	39
7	Conclusion	43
A	Fault-Tolerance of Fiber Transversal Gates	46
B	Example QASM	47

1 Introduction

Given that you have protected your fragile quantum information from the world, how do you then gain access to and thereby manipulate this quantum information? This is the fundamental trade-off in the theory of quantum error correction. While the primary goal is to shield quantum data from errors, the challenge lies in devising methods to interact with and utilize this protected information for computational tasks. Achieving this balance between protection and accessibility is essential for realizing the full potential of quantum error correction in practical applications.

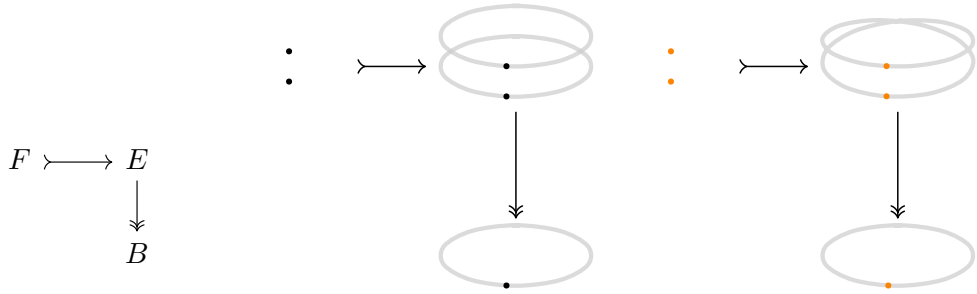
One of the best techniques for circumventing this problem is to apply quantum gates *transversally* between copies of the same quantum code, see [18] §5.3. We view this copying process as analogous to the concept of *covering spaces*. The *base code* C is *covered by* the *total code* $C \oplus C$. (Here we are using additive \oplus notation.) Every qubit j in C is *covered by* two qubits in $C \oplus C$. These two qubits are called the *fiber over* j . Transversal gates operate separately on each fiber in the cover. We call these gates *fiber transversal*. See Fig. 1.

Making copies like this we only get trivial covering spaces; a cartesian product of a particular fiber $\mathbf{2}$ with the code C giving $\mathbf{2} \times C = C \oplus C$. In this work we construct a double cover called the *symplectic double* of C and denoted $\mathfrak{D}(C)$. This cover is trivial when C is a CSS code but becomes non-trivial otherwise.

A key idea is *functoriality*: logical Clifford operations on the base code can be lifted to logical operations on the total code. In the symplectic double we often get an interesting set of fault-tolerant Clifford gates. When the base Clifford gate is a product of single qubit Cliffords, the lifted gate is fiber transversal, and these are fault-tolerant for the same reason as in the trivial case: locally the cover is trivial.

Of particular interest to us is a family of topological codes defined on 3- and 4-valent graphs inscribed on compact surfaces of arbitrary genus. We call these *genon codes*. The graph determines the code up to local Clifford equivalence, with twists or *genons* associated to the 3-valent vertices. This family of topological codes includes surface codes, toric codes, hyperbolic surface codes, $XZZX$ codes, the $[[5, 1, 3]]$ code. See Fig. 2.

Applied to genon codes, the symplectic double corresponds to a topological double cover, which is a discrete (combinatorial) version of branched double covers of Riemann surfaces. Counting the genus of the base space and the double cover space fixes the number of genons



- (i) The *fiber* F is included into the *total space* E which projects down onto the *base space* B .
- (ii) A trivial double cover is just two copies of the base space, or the cartesian product of the base with the fiber.
- (iii) A twisted double cover: locally this looks like a trivial double cover, globally there is a twist.

Figure 1: A schematic depiction of the symplectic double as a covering space. (ii) Given any CSS code C , the two copies $C \oplus C$ give a trivial double cover of C , and we have a logical transversal CX gate applied to the *fibers* of the cover. (iii) When C is not a CSS code we find there is a twisted double cover $\mathfrak{D}(C)$ that also supports Clifford gates applied to the fibers.

in the base, and this is the origin of the term *genon*. These are also called twists, dislocations or defects in the literature [5, 4, 22, 10, 37, 6].

1.1 Outline

We discuss the underlying theory of two-dimensional topological order with $D(\mathbb{Z}_2)$ anyon excitations in §2.1. This calculus is divorced from the microscopic details of the system, so we don't need to take into account any qubit or stabilizer structure, and can instead focus on the large-scale topological properties of the system. Crucially this phase has one non-trivial symmetry which we denote using one-dimensional domain walls. The endpoints of domain walls are the genons, and by braiding these we can perform logical Clifford gates.

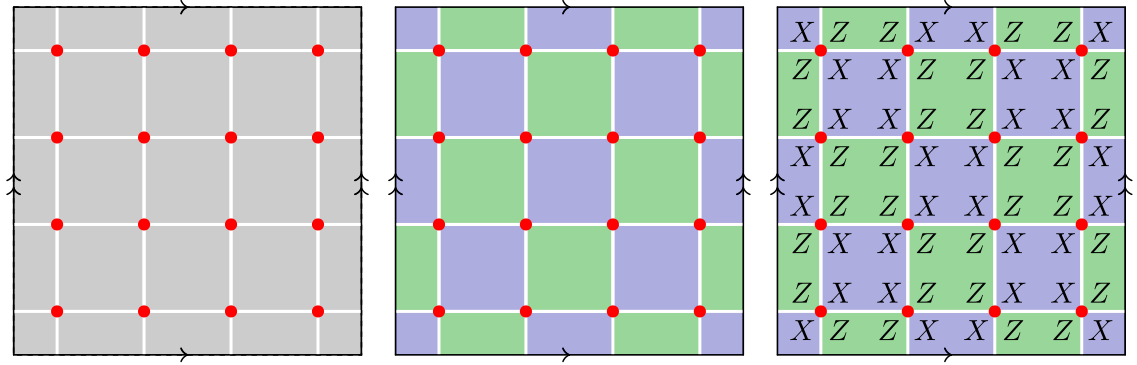
The symmetry exhibited by domain walls has another incarnation as precisely the data needed to construct a *double cover* of our two-dimensional manifold, or *Riemann surface* §2.1.3. Topological operations in the base space, such as braiding genons, will then lift functorially to topological operations in the total space, such as Dehn twists.

We review background on quantum stabilizer codes and notation in §2.3 and then introduce the *symplectic double* construction in §3, and show how logical Clifford gates on the base code lift functorially to logical Clifford gates on the total code §3.1, as well as their fault-tolerance. These lifted Clifford gates lie in the phase-free ZX -calculus.

We introduce our formalism for topological codes with genons in §4.1. These are called *genon codes*, and come with a theory of logical string operators which is invariant under local Clifford operations §4.2, as well as rules for decoration by *domain walls* §4.3. When a genon code has no unnecessary Y operators the symplectic double will also be a genon code §4.4.

In §5 we go through a series of example genon codes and symplectic doubles. These have interesting Clifford gates, which we call *genon protocols*. The smallest interesting example is a $[[4, 1, 2]]$ genon code with 4 genons, whose symplectic double is a $[[8, 2, 2]]$ toric code. We show how braiding these four genons gives a protocol for implementing the single qubit Clifford group, as well as Dehn twists on the $[[8, 2, 2]]$ toric code.

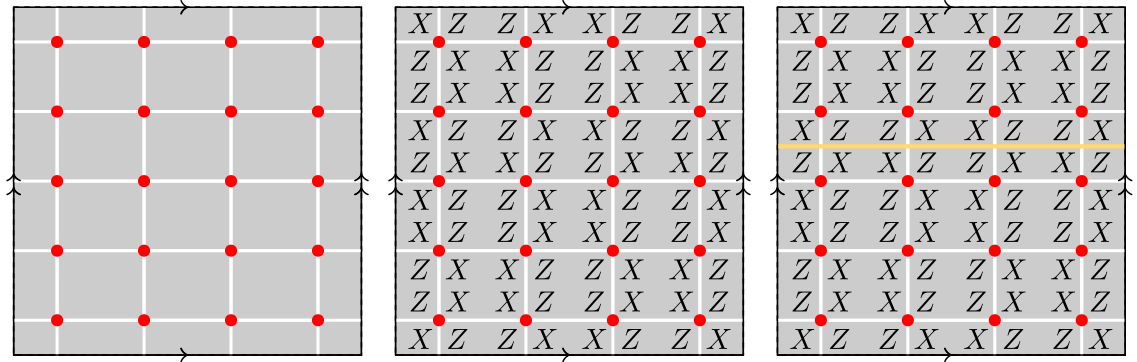
We experimentally demonstrate three different protocols on Quantinuum's H1-1 trapped-



(i) A graph Γ on a torus with 16 vertices in red, 32 edges in white and 16 faces in grey.

(ii) The faces of Γ are bicolourable: we paint each face with one of two colours blue or green such that neighbouring faces have different colours.

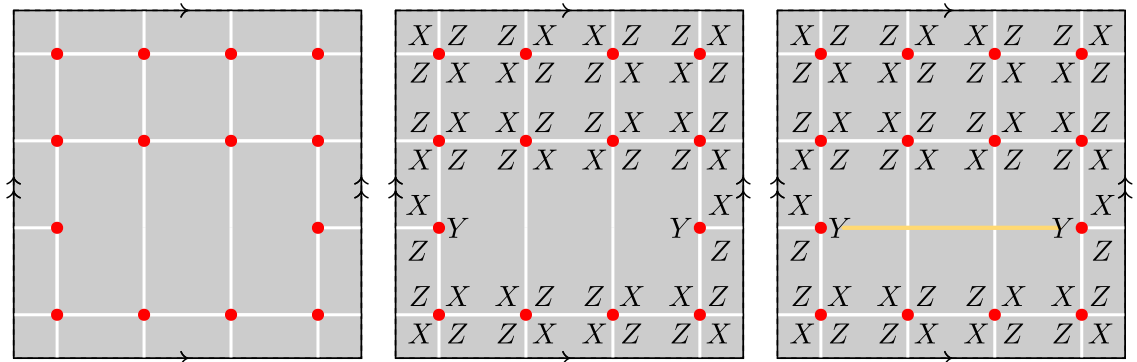
(iii) We associate a qubit with each vertex and a stabilizer with each face. Using the bicolouring to determine X or Z type stabilizers we recover the usual (rotated) toric code.



(iv) The graph Γ has an odd number of faces in the vertical direction which prohibits bicolouring the faces.

(v) We can still define a quantum code as above but some stabilizers are both X and Z type and this is a non-CSS code.

(vi) We insert a *domain wall* separating or resolving the X and Z sectors appropriately.



(vii) This graph Γ has two trivalent vertices.

(viii) We place XYZ around trivalent vertices.

(ix) Here the domain wall connects the two trivalent vertices.

Figure 2: Constructing a rotated toric code on a graph with bicolourable faces (i)-(iii). The frustrated bicolourability of Γ is related to domain walls (iv)-(vi). Trivalent vertices, or *genons*, are another reason bicolourability is frustrated (vii)-(ix).

ion quantum computer, including genon braiding on the $[[4, 2, 2]]$ code, Dehn twists on the $[[8, 2, 2]]$ code and a lifted Clifford gate on the $[[10, 2, 3]]$ code §6. Such experiments are a “proof-of-principle,” demonstrating that the gates arising from the procedures can be realized on modern quantum computers. We conclude in §7.

We aim to use a consistent colour scheme as an aid to recognizing the same concept as it appears in seemingly different guises. Qubits are red dots, X -type string operators are blue, and Z -type string operators are green. This blue/green colour scheme also applies to ZX -calculus. The symmetry that swaps blue and green is coloured yellow and occurs both as domain walls and the Hadamard gate.

Finally, there are several *Claims* in this work which can be taken to be either unproven theorems, or conjectures.

1.2 Related work

This work necessarily treads a well-worn path, and we cite some of the work to be found on this path here.

- This work is a continuation of the first author’s work on ZX -dualities and folding [8]: “fold-transversal” logical gates are examples of what is here called fiber transversal.
- The symplectic double construction also appears in [29], where it is applied to subsystem codes.
- A particular example of a genon code without any genons is the $XZZX$ code [7], and the $[[5, 1, 3]]$ code.
- Surface codes are an example of genon codes on a sphere: in [19] they consider modifying such face-bicolourable 4-valent graphs to support 3-valent dislocations, as well as qudit generalizations.
- Another treatment of surface codes and twists is found in [6], where the focus is on 2+1 dimension circuit construction.
- The family of genon codes defined in this work overlaps and is inspired by the graph-based formalism of Sarkar-Yoder [33]. They were the first to identify the well-known $[[5, 1, 3]]$ as a member of a family of topological codes defined on a torus. In the Sarkar-Yoder formalism they take genons (branch points) to occur precisely at the trivalent (or odd-valent) vertices, and so obtain a deficiency in the vertex count of the double cover (see proof of Thm. 4.9). In this work we take genons (branch points) to occur on faces near to the trivalent vertices, giving exactly twice the number of vertices in the double cover (and a deficiency in the doubled faces). This works better for our purposes as we then find a connection with the symplectic double, from which our other code constructions follow. The Sarkar-Yoder formalism takes the branch cuts between genons to consist of paths along edges of the graph with endpoints at the trivalent vertices. These paths are called defect lines and they show how these relate to a bicolor (or checkerboard) on the faces. In this work we take branch cuts to be paths perpendicular to the edges, which then give the *domain walls* for the underlying topological order. The Sarkar-Yoder formalism also contains a doubling construction in §4.3, that reproduces our symplectic double when there are no genons present. For example, the Sarkar-Yoder double of the $[[5, 1, 3]]$ code is the $[[10, 2, 3]]$ toric code.

- A description of Dehn twists on topological codes appears in [9], §4.2.
- In [28] Appendix D, they describe a protocol for instantaneous Dehn twists involving permutations of qubits followed by Pachner moves. These Pachner moves are implemented using constant depth CX circuits and are designed to re-triangulate the code lattice after performing the qubit permutation. Their work is developed further in [38] where more protocols for performing braids of defects (genons) and Dehn twists are given.
- Further discussion on Clifford gates on topological codes is in [10, 27].

2 Background

2.1 $D(\mathbb{Z}_2)$ topological order

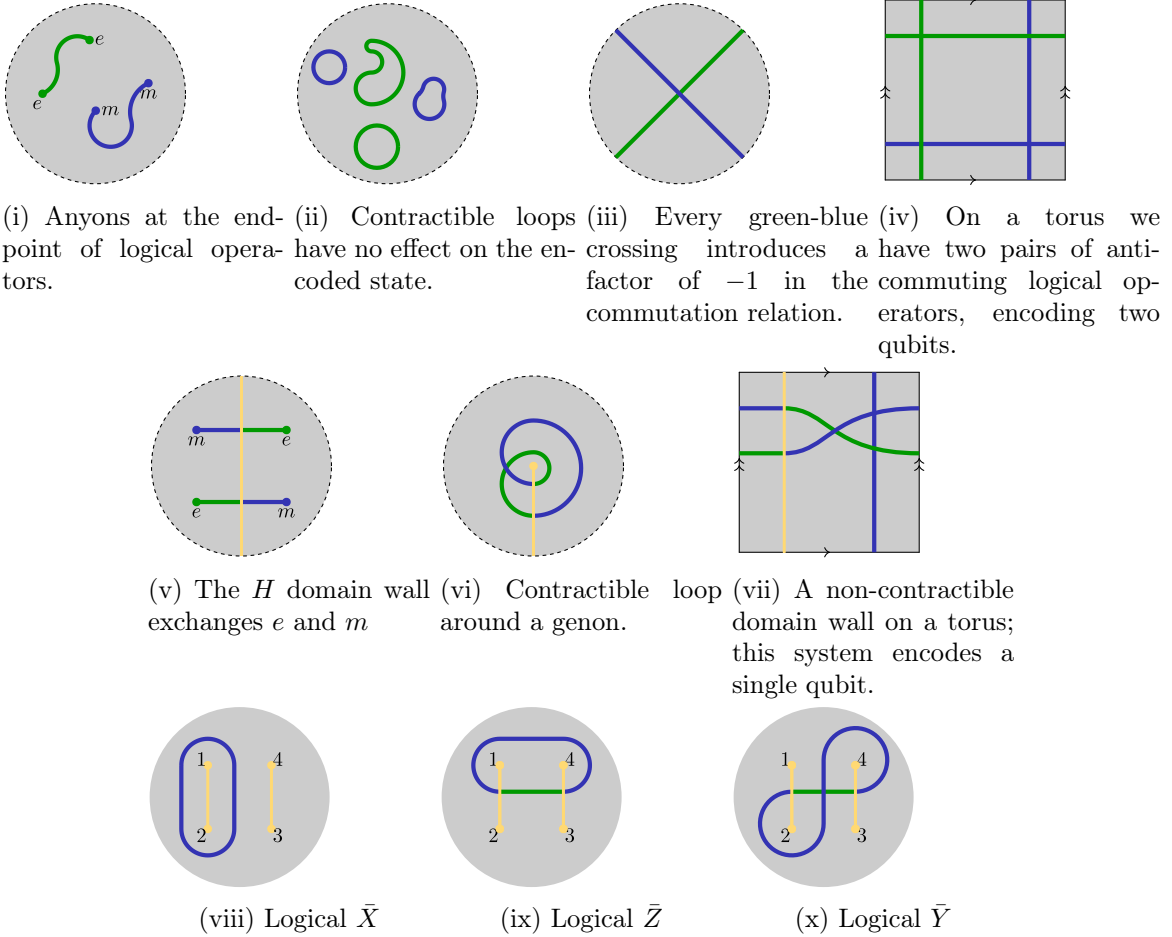


Figure 3: String operators are coloured blue and green, which are X - and Z -type respectively. The H domain wall is a yellow string, whose (any) endpoints are called genons. (viii)-(x): A sphere supporting four genons encodes one logical qubit.

In this section, we briefly discuss the theory of $D(\mathbb{Z}_2)$ topological order, describing anyon

statistics through the use domain walls, defects and genons. For a more in depth and accessible introduction we recommend [10], as well as [3] §VI and [12].

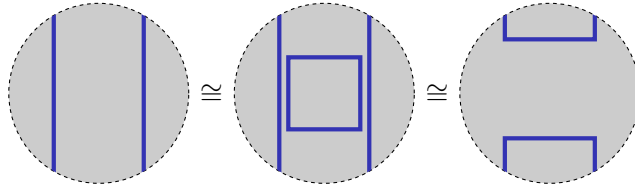
To start, consider an abelian anyon model with four anyon types: *vacuum*, *electric*, *magnetic* and *electromagnetic* anyons. We denote these ι, e, m, ε respectively (See Fig. 3). Fusion rules describe how pairs of anyons combine to form other anyons. These rules are as follows:

$$\begin{aligned} \iota \times a &= a \times \iota = a \quad \text{for all anyon labels } a \\ e \times e &= m \times m = \varepsilon \times \varepsilon = \iota \\ e \times m &= m \times e = \varepsilon \\ e \times \varepsilon &= \varepsilon \times e = m \\ m \times \varepsilon &= \varepsilon \times m = e \end{aligned}$$

We can describe the path of an anyon on a topological surface by a string operator whose end points are the anyons. When these string operators are closed, they are the logical operators of the topological code. Here we adopt the convention that blue strings connecting two e anyons are X -type operators and green strings connecting two m anyons are Z -type operators. These strings can cross and annihilate ends points following the fusion rules (see Fig. 3).

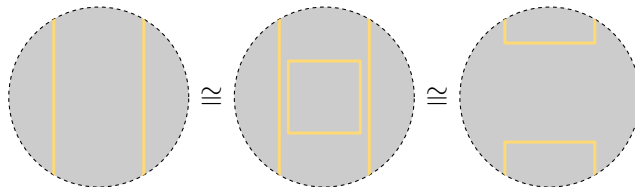
This topological order supports two automorphisms: the trivial automorphism and the automorphism that swaps e and m . These automorphisms occur when anyons cross a boundary, or *domain wall*, that separates regions. The trivial automorphism is realized by anyons crossing a trivial domain wall, while the $e - m$ swapping automorphism occurs when anyons cross a non-trivial domain wall. The endpoints of these non-trivial domain walls we call *genons*.

Because $m \times m = \iota$ and $e \times e = \iota$ the associated string operators are self-inverse. In other words, two copies of the same colour string can be erased:

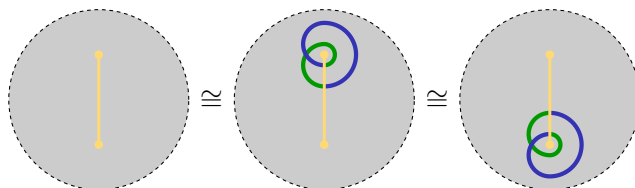


and similarly for Z -type string operators.

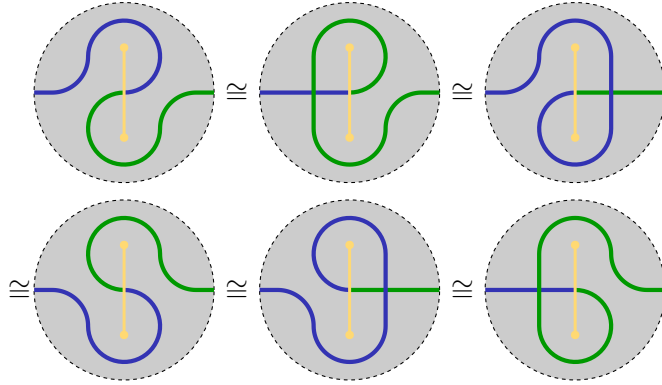
The H domain wall exchanges $e \leftrightarrow m$ and so is also self-inverse but for a different reason:



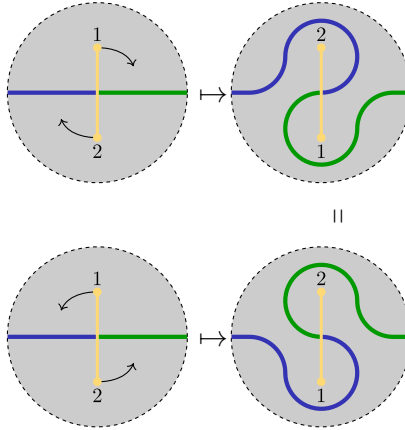
Contractible loops around genons



imply the following equations



We see from this that performing a *braid* between two genons has the same result clockwise versus anti-clockwise:



Therefore we can refer to a braid of genons by the underlying permutation of the genon labels.

Connecting these concepts to the language of the stabilizer formalism (see §2.3), we record the following dictionary:

<u>$D(\mathbb{Z}_2)$ topological order</u>	<u>Quantum stabilizer codes</u>
X/Z -type string operator	X/Z -type logical operator
contractible string operator	stabilizer
e/m anyon	frustrated X/Z -type stabilizer

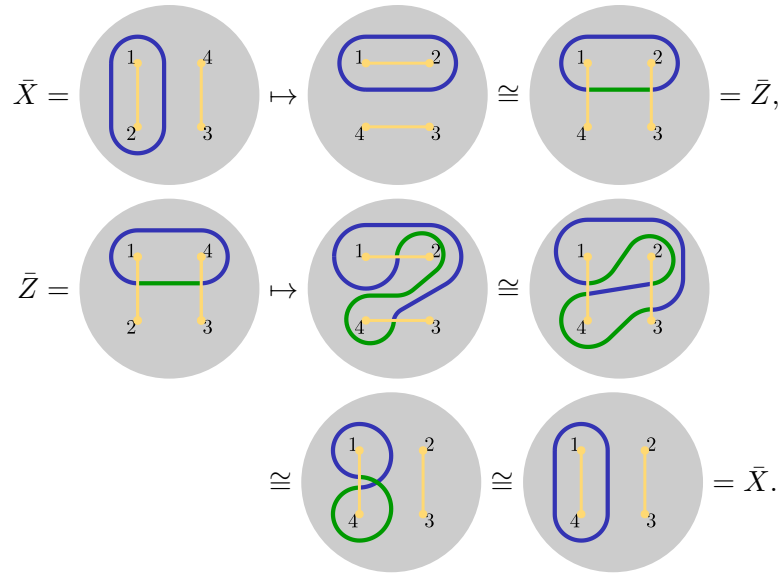
2.1.1 Example in genus zero

So far we have only discussed *local* rules for anyon calculations, as depicted by the dashed line surrounding grey regions. In this section we consider the effect that the *global* topology has.

A sphere with four genons (two domain walls), encodes one logical qubit, Fig. 3. By topological deformation, we braid these genons. Here we number the genons 1, 2, 3, 4 and see the action on the logical operators as we perform these braids.

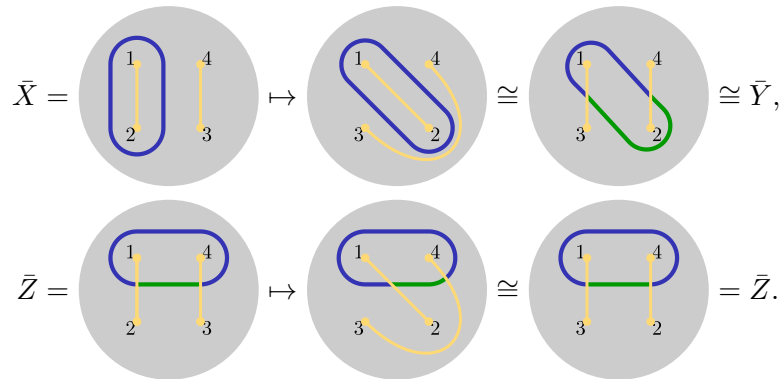
The first gate we try is given by the permutation operator $\sigma = (1, 4, 3, 2)$. This is swapping

genons 2 and 4, and we show a clockwise braid of these two genons:



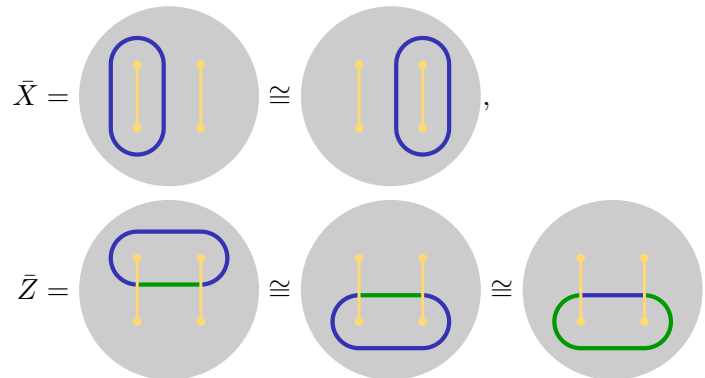
And therefore this braid implements a logical H gate.

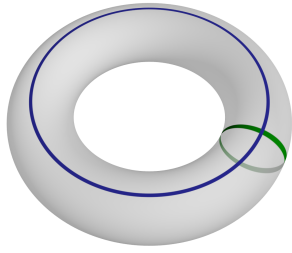
The next permutation we examine is $\sigma = (1, 3, 2, 4)$ which swaps genons 2 and 3.



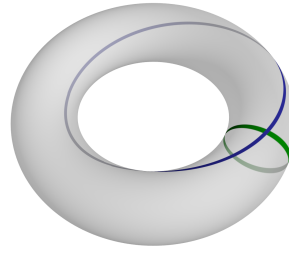
And this gives a logical S gate.

Finally we note that the two permutations $(2, 1, 4, 3)$ and $(3, 4, 1, 2)$ leave the logical operators invariant. This is because we are working on a sphere and can drag operators around the back of the sphere:





(i) The torus with an anti-commuting pair of logical operators.



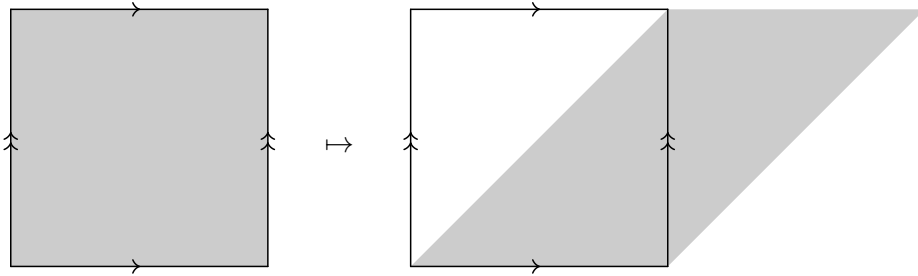
(ii) A Dehn twist introduces a full rotation in the torus. Here we see the blue string operator now winds around the back of the torus.

Figure 4: A Dehn twist on a torus.

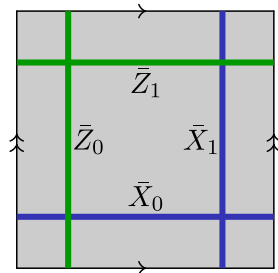
We will show in §5 below a minimal implementation of these gates in a four qubit quantum code.

2.1.2 Dehn twists

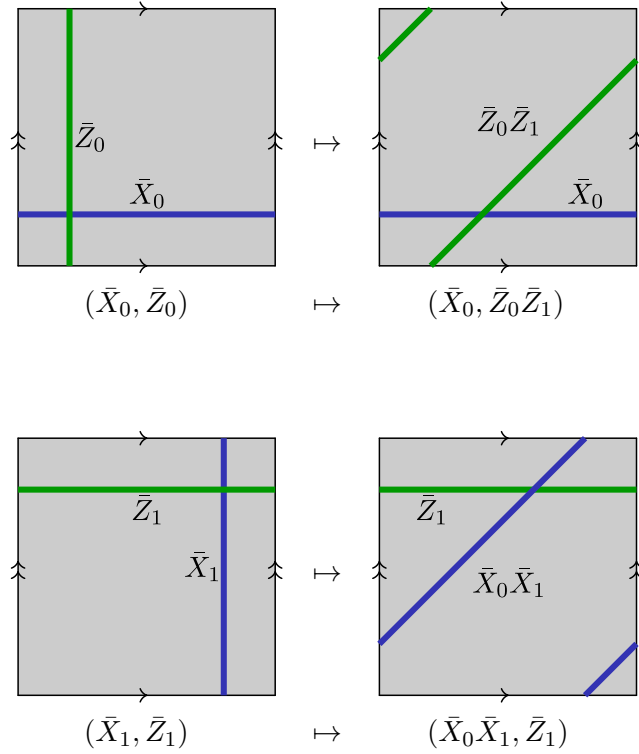
On a genus zero surface (sphere) the only non-trivial homeomorphisms up to isotopy are the genon braids. On a higher genus surface we have many more non-trivial homeomorphisms. A *Dehn twist* on a torus T is a homeomorphism of the torus that introduces a global twist in the torus, see Fig. 4. A horizontal Dehn twist is implemented as a linear shear operation, up to periodic boundary conditions:



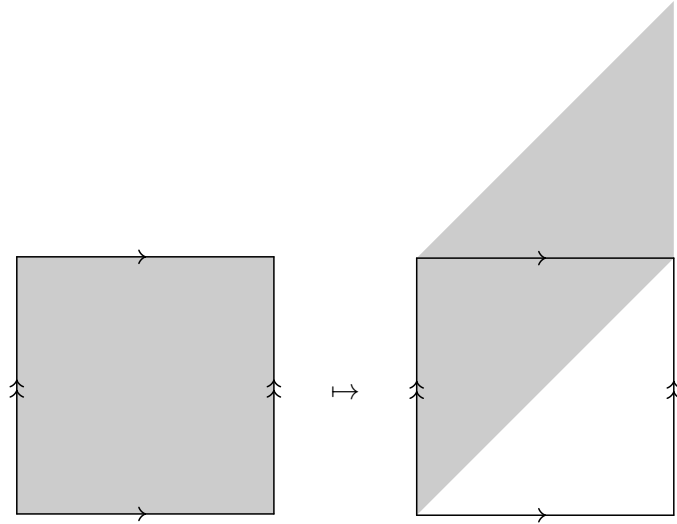
Now we compute the action of this horizontal Dehn twist on the logical operators. A complete set of logical operators is given in anti-commuting pairs (\bar{X}_0, \bar{Z}_0) and (\bar{X}_1, \bar{Z}_1) :



The action of a horizontal Dehn twist is then found to be



and therefore this Dehn twist implements logical $CX_{1,0}$ with control qubit 1 and target qubit 0. A similar calculation shows that the vertical Dehn twist



implements a logical $CX_{0,1}$. The combination of these two logical gates generates the group $\text{GL}(2, \mathbb{Z}_2)$ which is isomorphic to the permutation group S_3 of order 6.

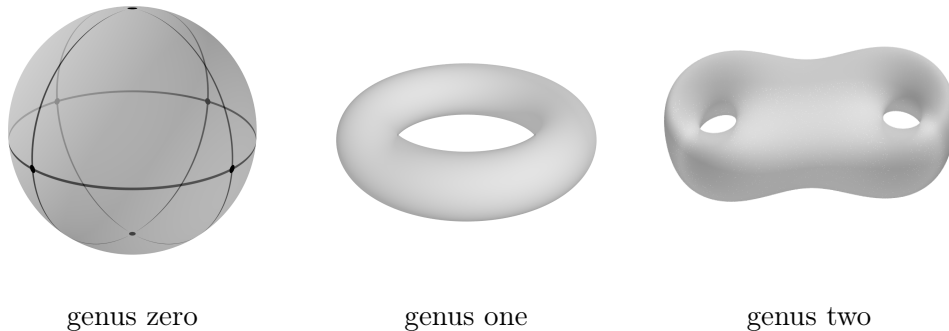
These two Dehn twists are known to implement the *mapping class group* of the torus [16]. The mapping class group of a surface is the group of isotopy classes of homeomorphisms of the surface.

2.1.3 Riemann surfaces and double covers

In this section we re-interpret the above theory of $D(\mathbb{Z}_2)$ topological order using the language of Riemann surfaces. Loosely speaking, if domain-walls correspond to passing between the normal world and a “bizarro” world, then why don’t we interpret this literally? In other words, take two copies of the topological phase and cut/glue them together appropriately, along the domain walls. This motivates the following consideration of *branched double covers*.

Topologically, there are only two ways to double cover a circle, which is the only compact connected one-dimensional manifold, see Fig. 1. When we do this with compact surfaces things get much more interesting. See the textbook [17] §1.2.5.

Compact oriented connected topological surfaces are characterized by their *genus*, which counts the number of “holes”:



The genus zero surface is a sphere, and we have inscribed on it $v = 6$ vertices, $e = 12$ edges joining vertices, and $f = 8$ faces, thus giving the *Euler character*

$$\chi = v - e + f = 6 - 12 + 8 = 2.$$

In general, for a genus g surface we have that $\chi = 2 - 2g$. The Euler character of a surface constrains what graphs we can inscribe on that surface.

Given a compact surface E that double covers a surface B ,

$$\begin{array}{c} E \\ \downarrow p \\ B \end{array}$$

the Euler characteristic $\chi(\cdot)$ satisfies the formula

$$\chi(E) = 2\chi(B)$$

If the cardinality of the fiber $p^{-1}(b)$ is 1 at a point $b \in B$ we say that the cover has a *branch point* at b . Such branch points introduce a correction into the formula for the Euler characteristic:

$$\chi(E) = 2\chi(B) + m$$

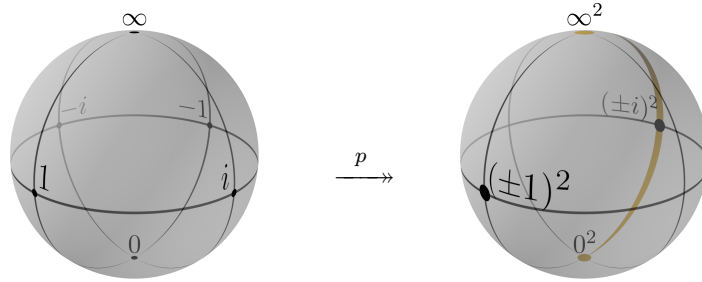
where m is the number of branch points. This is a special case of the more general Riemann-Hurwitz formula, see [17] Thm 1.76. In terms of the *genus* $g(\cdot)$ of the surfaces E and B , we

have

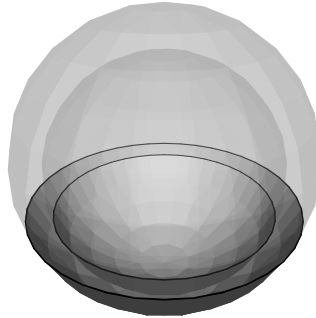
$$2g(E) - 2 = 2(2g(B) - 2) + m,$$

$$g(E) - 1 = 2g(B) - 2 + \frac{1}{2}m.$$

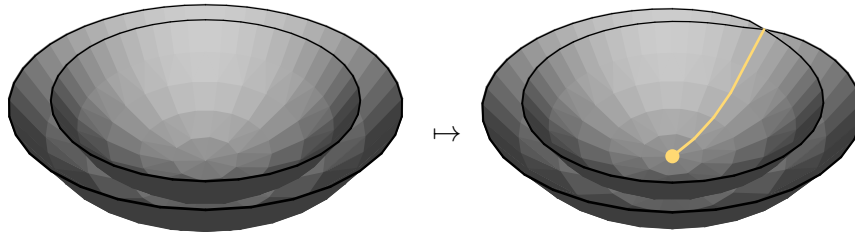
When the genus of both E and B is zero we find that $m = 2$. This cover is given by the double cover of the Riemann sphere, or extended complex plane, under the function $f(z) = z^2$. Most points, such as $1 = (\pm 1)^2$ and $-1 = (\pm i)^2$ are double covered by f , except for the $m = 2$ points at 0 and ∞ :



The yellow line is an arbitrary line connecting the two yellow branch points at $z = 0$ and $z = \infty$. We can construct these branched covers with some cutting and gluing. First we take two copies of the base space:



This is the trivial double cover of the base. Now focusing on the lower part of this figure:



This shows explicitly how domain walls and genres correspond to branches of double covers, and will motivate the development of the qubit theory below, see Fig. 8.

Here we tabulate values of m for various double covers:

$m = ?$	$g(E)=0$	$g(E)=1$	$g(E)=2$	$g(E)=3$	$g(E)=4$	$g(E)=5$
$g(B) = 0$	2	4	6	8	10	12
$g(B) = 1$		0	2	4	6	8
$g(B) = 2$				0	2	4
$g(B) = 3$						0

The interplay between the m branch points and the resulting genus of a double cover is the origin of the term *genon*. In summary, we have the following dictionary:

$D(\mathbb{Z}_2)$ topological order	<u>Riemann surfaces</u>
domain wall	branch cut
genon	branch point

2.2 ZX-calculus survival guide

The ZX-calculus is a notation for drawing quantum circuit diagrams [13, 35]. We draw circuits from right to left, in agreement with algebraic (Dirac) notation. The building blocks for this notation are wires, blue and green *spiders*, and the yellow Hadamard box. Such diagrams are examples of tensor networks. In this section we give a brief and incomplete introduction to this notation and how we compute with it.

ZX-diagram								
Dirac notation	$ 0\rangle$	$ 1\rangle$	$ +\rangle$	$ -\rangle$	$\langle 0 $	$\langle 1 $	$\langle + $	$\langle - $

ZX-diagram							
Gate	X	\sqrt{X}	\sqrt{X}^\dagger	H	Z	S	S^\dagger

ZX-diagram					
Gate	$CX_{0,1}$	$CX_{1,0}$	CZ	$CY_{0,1}$	$SWAP$

The definition of a blue or green *spider* with m outputs, n inputs and labelled with *phase* $a \in \mathbb{Z}/4$ is given by:

$$\begin{array}{c}
 \begin{array}{ccc}
 1 & \text{---} & 1 \\
 \vdots & & \vdots \\
 m & \text{---} & n
 \end{array} \\
 \begin{array}{c}
 \diagup \quad \diagdown \\
 \bullet \\
 \diagdown \quad \diagup \\
 a
 \end{array}
 \end{array}
 := |0\rangle^{\otimes m} \langle 0|^{\otimes n} + e^{2\pi i a/4} |1\rangle^{\otimes m} \langle 1|^{\otimes n}$$

$$\begin{array}{c}
 \begin{array}{ccc}
 1 & \text{---} & 1 \\
 \vdots & & \vdots \\
 m & \text{---} & n
 \end{array} \\
 \begin{array}{c}
 \diagup \quad \diagdown \\
 \bullet \\
 \diagdown \quad \diagup \\
 a
 \end{array}
 \end{array}
 := |+\rangle^{\otimes m} \langle +|^{\otimes n} + e^{2\pi i a/4} |-\rangle^{\otimes m} \langle -|^{\otimes n}$$

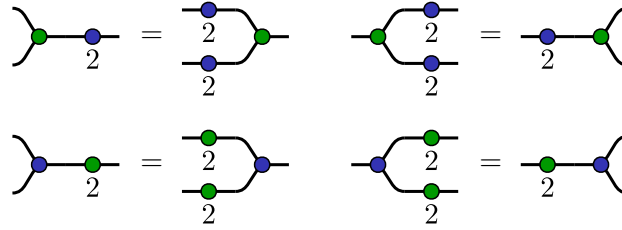
When the phase is zero we usually omit the phase label. ZX-diagrams without phase labels are called *phase-free*.

The most important equations for our purposes allow us to commute the Pauli X and Z operators through a circuit. When a phase 2 operator meets a spider of the same colour, it passes through freely:

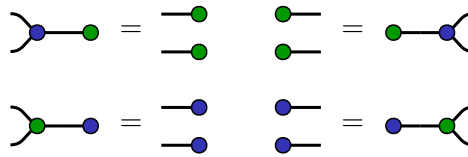
$$\begin{array}{ccccccc}
 \begin{array}{c} \text{---} \bullet \text{---} \\ \bullet \\ \text{---} \end{array} & = & \begin{array}{c} \text{---} \text{---} \\ \text{---} \bullet \text{---} \\ \bullet \\ \text{---} \end{array} & = & \begin{array}{c} \bullet \\ \text{---} \text{---} \\ \bullet \end{array} & \begin{array}{c} \text{---} \bullet \text{---} \\ \bullet \\ \text{---} \end{array} & = & \begin{array}{c} \text{---} \text{---} \\ \text{---} \bullet \text{---} \\ \bullet \\ \text{---} \end{array} & = & \begin{array}{c} \bullet \\ \text{---} \text{---} \\ \bullet \end{array}
 \end{array}$$

$$\begin{array}{ccccccc}
 \begin{array}{c} \text{---} \bullet \text{---} \\ \bullet \\ \text{---} \end{array} & = & \begin{array}{c} \text{---} \text{---} \\ \text{---} \bullet \text{---} \\ \bullet \\ \text{---} \end{array} & = & \begin{array}{c} \bullet \\ \text{---} \text{---} \\ \bullet \end{array} & \begin{array}{c} \text{---} \bullet \text{---} \\ \bullet \\ \text{---} \end{array} & = & \begin{array}{c} \text{---} \text{---} \\ \text{---} \bullet \text{---} \\ \bullet \\ \text{---} \end{array} & = & \begin{array}{c} \bullet \\ \text{---} \text{---} \\ \bullet \end{array}
 \end{array}$$

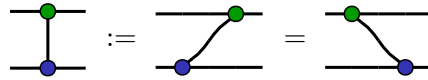
When a phase 2 operator meets a spider of the opposite colour, it is copied:



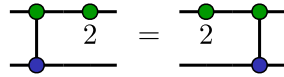
Similarly, states and effects get copied by spiders of the opposite colour:



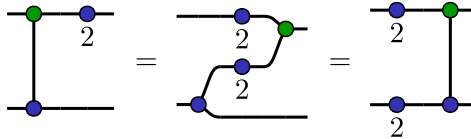
Spider legs are flexible, and this is how we justify the use of vertical wires in our ZX -diagrams. For example:



Using these rules we commute a Pauli Z operator on the control qubit of a CX :



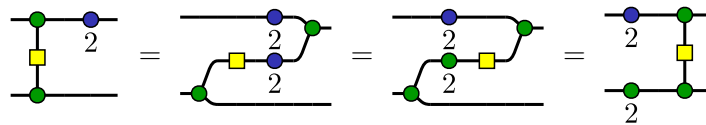
and a Pauli X operator,



This diagrammatic calculus is blue-green symmetric, and indeed, the ZX -calculus has a *Fourier duality* which implements this colour reversal:



Now we can commute the Pauli X operator through a CZ :



The Fourier duality plays a fundamental role in this work, and we make use of this blue-green-yellow colour scheme consistently to refer to this connection.

2.3 Quantum codes and symplectic geometry

In this section we recall basic facts about qubit stabilizer codes, their relation to symplectic geometry, and the Clifford group [11, 21].

Given a field \mathbb{F} , and integer $n \geq 0$, we define the *standard $2n$ -dimensional symplectic space* to be the $2n$ -dimensional vector space $\mathbb{F}^n \oplus \mathbb{F}^n$ with symplectic form

$$\Omega_n = \begin{pmatrix} 0 & I_n \\ -I_n & 0 \end{pmatrix}$$

where I_n is the $n \times n$ identity matrix. A vector $v \in \mathbb{F}^n \oplus \mathbb{F}^n$ is written as a block column matrix:

$$v = \begin{pmatrix} v_X \\ v_Z \end{pmatrix}$$

and we call v_X the X part of v and v_Z the Z part of v . Similarly for covectors and row matrices.

Given a vector v in the vector space \mathbb{F}^n we define the *weight* of v , denoted $w(v)$, to be the number of non-zero components of v . For a vector v in the standard symplectic space $\mathbb{F}^n \oplus \mathbb{F}^n$, we define the weight as

$$w(v) = w(v_X) + w(v_Z) - w(v_X \cdot v_Z),$$

where $v_X \cdot v_Z \in \mathbb{F}^n$ is the componentwise product of v_X and v_Z .

Let \mathbb{F}_2 be the finite field of order 2. Much of the theory below can be developed for other finite fields, but here we focus on the case \mathbb{F}_2 . We define a *quantum code* C to be an isotropic subspace $C \subset \mathbb{F}_2^n \oplus \mathbb{F}_2^n$ where $n \geq 0$ is an integer *number of qubits*. We also call C the *codespace*. Given such a code, the *logical space* is the coisotropic subspace given by:

$$C^\perp = \{v \in \mathbb{F}_2^n \oplus \mathbb{F}_2^n \mid v^\top \Omega_n C = 0\} \supset C.$$

The *parameters* $[[n, k, d]]$ of a quantum code C are: n the number of qubits, k the dimension of C^\perp/C , and d the minimum weight of $v \in C^\perp$ with $v \notin C$.

Quantum codes C can also be specified by a $m \times 2n$ (*parity*) *check matrix* \mathcal{H} . This is a full-rank matrix with $\mathcal{H} \Omega_n \mathcal{H}^\top = 0$. The codespace C is the rowspan of \mathcal{H} , and the logical space C^\perp is the kernel (nullspace) of the matrix $\mathcal{H} \Omega_n$. We write such a check matrix in block form $\mathcal{H} = (\mathcal{H}_X \mathcal{H}_Z)$ where \mathcal{H}_X and \mathcal{H}_Z are $m \times n$ matrices. Expanding the isotropic condition we find the equivalent statement

$$\mathcal{H}_X \mathcal{H}_Z^\top - \mathcal{H}_Z \mathcal{H}_X^\top = 0.$$

Given a quantum code $C \subset \mathbb{F}_2^n \oplus \mathbb{F}_2^n$ we say that C is *CSS* when we have the direct sum decomposition $C = C_X \oplus C_Z$ with $C_X \subset \mathbb{F}_2^n$ and $C_Z \subset \mathbb{F}_2^n$. Equivalently, C is CSS when it has a check matrix of the form

$$\mathcal{H} = (\mathcal{H}_X \mathcal{H}_Z) = \begin{pmatrix} \mathcal{H}'_X & 0 \\ 0 & \mathcal{H}'_Z \end{pmatrix}.$$

In other words, \mathcal{H}_X and \mathcal{H}_Z can be written without any nonzero rows in common.

We will make use of *Pauli operator* notation: for a vector $v \in \mathbb{F}_2^n \oplus \mathbb{F}_2^n$, with components $(v_1, \dots, v_n, v_{n+1}, \dots, v_{2n})$ we write this as a length n string (n -tuple) of symbols I, X, Y, Z with i -th entry given by

$$\begin{cases} I & \text{if } v_i = 0, v_{n+i} = 0, \\ X & \text{if } v_i = 1, v_{n+i} = 0, \\ Z & \text{if } v_i = 0, v_{n+i} = 1, \\ Y & \text{if } v_i = 1, v_{n+i} = 1. \end{cases}$$

We also use the dot $.$ in place of I . For example, the vector $(1011) \in \mathbb{F}_2^2 \oplus \mathbb{F}_2^2$ has Pauli operator YZ . The subspace of $\mathbb{F}_2^n \oplus \mathbb{F}_2^n$ spanned by v_i, v_{n+i} is the i -th *qubit*. We declare two codes C and C' to be isomorphic $C \cong C'$ when they are the same up to permutation of qubits.

For an example of a $[[4, 1, 2]]$ quantum code $C \subset \mathbb{F}_2^4 \oplus \mathbb{F}_2^4$ we have the parity check matrix and corresponding Pauli operator notation:

$$\mathcal{H} = \left(\begin{array}{ccc|ccc} 11 & . & . & . & 11 & . \\ . & 11 & . & . & . & 11 \\ . & . & 11 & | & 1 & . & . & 1 \end{array} \right) = \begin{pmatrix} XY & Z & . \\ . & XY & Z \\ Z & . & XY \end{pmatrix}.$$

We have a vertical line separating the \mathcal{H}_X and \mathcal{H}_Z blocks, and the dot notation is for zero or I entries. An example of a CSS code $C \subset \mathbb{F}_2^8 \oplus \mathbb{F}_2^8$ with parameters $[[8, 2, 2]]$ is given by

$$\mathcal{H} = \left(\begin{array}{cccc|cccc} 11 & . & . & . & . & . & . & . \\ . & 11 & . & . & . & . & . & . \\ . & . & 11 & . & . & . & . & . \\ . & . & . & . & 11 & . & . & . \\ . & . & . & . & . & 11 & . & . \\ . & . & . & . & . & . & 11 & . \\ . & . & . & . & . & . & . & 11 \end{array} \right) = \begin{pmatrix} XX & . & . & . & XX & . \\ . & XX & . & . & . & XX \\ . & . & XX & X & . & . & X \\ . & Z & Z & . & Z & Z & . \\ . & . & Z & Z & . & Z & Z \\ Z & . & . & Z & . & . & Z & Z \end{pmatrix}.$$

These two examples are chosen for a reason: the parity check matrix of the $[[8, 2, 2]]$ code contains two copies of the parity check matrix of the $[[4, 1, 2]]$ code. This *symplectic double* procedure is the subject of §3 below.

2.3.1 The qubit Clifford and Pauli groups

The n -qubit *Pauli group*, also called the *Heisenberg-Weyl group*, $\text{Pauli}_2(n)$ is a subgroup of the unitary group $U(2^n)$ generated by n -fold tensor products of the matrices

$$iI = \begin{pmatrix} i & 0 \\ 0 & i \end{pmatrix}, \quad X = \begin{pmatrix} 0 & 1 \\ 1 & 0 \end{pmatrix}, \quad Z = \begin{pmatrix} 1 & 0 \\ 0 & -1 \end{pmatrix}.$$

This group has order given by

$$|\text{Pauli}_2(n)| = 4 \cdot 4^n$$

and the center $\mathcal{Z}(\text{Pauli}_2(n)) \cong \mathbb{Z}/4$ is generated by i . The quotient $\text{Pauli}_2(n)/\mathcal{Z}(\text{Pauli}_2(n))$ is isomorphic to (the additive group of) the \mathbb{F}_2 -vector space \mathbb{F}_2^{2n} . We write this as the short exact sequence:

$$\mathbb{Z}/4 \hookrightarrow \text{Pauli}_2(n) \twoheadrightarrow \mathbb{F}_2^{2n}.$$

The 2-cocycle for this central extension is a function $\beta : \mathbb{F}_2^{2n} \times \mathbb{F}_2^{2n} \rightarrow \mathbb{Z}/4$ satisfying

$$\beta(v, w) \pmod{2} = \langle v, w \rangle,$$

for all $v, w \in \mathbb{F}_2^{2n}$. Here we write $\langle v, w \rangle$ for the symplectic inner product on \mathbb{F}_2^{2n} . See [23] §3.3.1.

The n -qubit Clifford group can be defined to be the normalizer of $\text{Pauli}_2(n)$ in the unitary group $U(2^n)$. This is an infinite group, however for our purposes we will be using the following finite subgroup as our definition of the n -qubit *Clifford group*. This is generated from scalar and matrices,

$$\omega, \quad H = \frac{1}{\sqrt{2}} \begin{pmatrix} 1 & 1 \\ 1 & -1 \end{pmatrix}, \quad S = \begin{pmatrix} 1 & 0 \\ 0 & i \end{pmatrix}, \quad CZ = \begin{pmatrix} 1 & 0 & 0 & 0 \\ 0 & 1 & 0 & 0 \\ 0 & 0 & 1 & 0 \\ 0 & 0 & 0 & -1 \end{pmatrix}$$

using multiplication and tensor products. For $n \geq 0$, this group is denoted $\text{Cliff}_2(n)$ and has order given by

$$|\text{Cliff}_2(n)| = 8 \prod_{j=1}^n 2(4^j - 1)4^j.$$

This sequence begins as 8, 192, 92160, 743178240, ... and is sequence A003956 in the OEIS. These matrices have elements in the ring $\mathbb{Q}[1^{1/8}]$. See [34], Figure 8, for an abstract presentation of the Clifford group(s) in terms of generators and relations.

The reference [23] uses a slightly different definition of the Clifford group which is an index two subgroup of $\text{Cliff}_2(n)$, §4.1.2. ¹ This is done by altering the definition of the Hadamard. The generators are:

$$i = \omega^2, \quad \omega H = \frac{i+1}{2} \begin{pmatrix} 1 & 1 \\ 1 & -1 \end{pmatrix}, \quad S, \quad CZ.$$

The generated matrices have elements in the ring $\mathbb{Q}[i]$. We call this group the n -qubit *semi-Clifford group*, denoted $\text{SemiCliff}_2(n)$. The OEIS notes that the order of these groups A027638 is also the order of a unitary group acting on Siegel modular forms.

The center $\mathcal{Z}(\text{Cliff}_2(n))$ is isomorphic to $\mathbb{Z}/8$, and we define the quotient group to be the *affine symplectic group* over \mathbb{F}_2 :

$$\text{ASp}(2n, \mathbb{F}_2) := \text{Cliff}_2(n) / \mathcal{Z}(\text{Cliff}_2(n)).$$

Warning: for $n > 1$, this group is not (!) isomorphic to the expected definition of the affine symplectic group which is the semidirect product $\text{Sp}(2n, \mathbb{F}_2) \ltimes \mathbb{F}_2^{2n}$. This is a peculiar consequence of the dimension of our qubit space which is even. The story is much simpler for odd prime-dimensional qudits.

Combining the above, we have the following commutative diagram of group homomorphisms, where every row and column is short exact:

$$\begin{array}{ccccc} \mathbb{F}_2^{2n} & \hookrightarrow & \text{ASp}(2n, \mathbb{F}_2) & \twoheadrightarrow & \text{Sp}(2n, \mathbb{F}_2) \\ \uparrow & & \uparrow & & \uparrow \\ \text{Pauli}_2(n) & \hookrightarrow & \text{Cliff}_2(n) & \twoheadrightarrow & \text{Mp}(2n, \mathbb{F}_2) \\ \uparrow & & \uparrow & & \uparrow \\ \mathbb{Z}/4 & \hookrightarrow & \mathbb{Z}/8 & \twoheadrightarrow & \mathbb{Z}/2 \end{array}$$

Here $\text{Mp}(2n, \mathbb{F}_2)$ is the metaplectic group over \mathbb{F}_2 . This suggests that the Clifford group is, or should be called, the affine metaplectic group. See also [20].

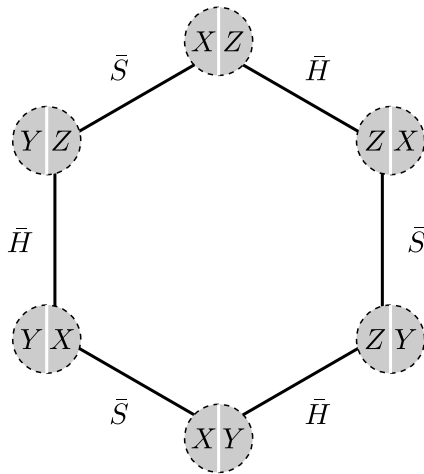


Figure 5: Here we record the action of single qubit Clifford operators S and H on anti-commuting pairs of Pauli operators. We notate the action via the barred operators \bar{S} and \bar{H} and we see that $\bar{S}\bar{H}\bar{S} = \bar{H}\bar{S}\bar{H}$.

In summary, the action of the Clifford group on the Pauli group by conjugation is, up to phases, represented by the symplectic group.

If we omit the entangling gate CZ from the list of generators of the Clifford group, we get the *local Clifford group*. As symplectic matrices, this is generated by n -fold direct sums of the \mathbb{F}_2 matrices

$$\bar{H} = \begin{pmatrix} 0 & 1 \\ 1 & 0 \end{pmatrix}, \quad \bar{S} = \begin{pmatrix} 1 & 0 \\ 1 & 1 \end{pmatrix}.$$

On a single qubit this group is $\text{Sp}(2, \mathbb{F}_2)$ which is isomorphic to the permutation group on three elements S_3 . See Fig. 5.

Lemma 2.1. The n -qubit local Clifford group preserves the parameters $[[n, k, d]]$ of a quantum code.

Proof. The Clifford group preserves the parameters n and k of any quantum code C . The local Clifford group preserves the weight of any vector $v \in \mathbb{F}_2^n \oplus \mathbb{F}_2^n$ and in particular will preserve the weight of any codeword in C , thereby preserving the parameter d . \square

3 The symplectic double

Given a vector space V over a field \mathbb{F} , we construct a symplectic space $\mathfrak{D}(V) := V \oplus V^*$ with symplectic form:

$$\begin{aligned} \Omega : \mathfrak{D}(V) \otimes \mathfrak{D}(V) &\rightarrow \mathbb{F} \\ (v \oplus c, u \oplus d) &\mapsto d(v) - c(u). \end{aligned}$$

Moreover, the assignment

$$\mathfrak{D}(V) = V \oplus V^*$$

¹there's a typo in eq. (4.12)

is *functorial*, which means that given invertible $f : V \rightarrow V$, we have that

$$\mathfrak{D}(f) := f \oplus (f^{-1})^* \quad (1)$$

is a symplectic map on $\mathfrak{D}(V)$:

$$\begin{aligned} & \Omega((f \oplus (f^{-1})^*)(v \oplus c), (f \oplus (f^{-1})^*)(u \oplus d)) \\ &= \Omega(f(v) \oplus cf^{-1}, f(u) \oplus df^{-1}) \\ &= d(v) - c(u) \\ &= \Omega(v \oplus c, u \oplus d). \end{aligned}$$

and also that $\mathfrak{D}(\cdot)$ preserves composition. In other words, we have a group homomorphism:

$$\mathfrak{D}(\cdot) : \text{GL}(V, \mathbb{F}) \rightarrow \text{Sp}(\mathfrak{D}(V), \mathbb{F}) \quad (2)$$

and this homomorphism is injective.

When V itself is symplectic, with symplectic form Ω_0 , we have an isomorphism

$$\begin{aligned} V &\xrightarrow{\cong} V^* \\ v &\mapsto \Omega_0(v, _). \end{aligned}$$

which we use in the definition of $\mathfrak{D}(\cdot)$, as the following lemma shows. This lemma is key to the construction of fault-tolerant Clifford gates on doubled codes.

Lemma 3.1. (*Functoriality*) Given symplectic space (V, Ω_0) with n -dimensional isotropic subspace $U \subset V$ then $\mathfrak{D}(U) := U \oplus \Omega_0(U, _)$ is a $2n$ -dimensional isotropic subspace of $\mathfrak{D}(V)$. Moreover, given a symplectic map $f : V \rightarrow V$ that preserves U as a subspace $f(U) = U$, then $\mathfrak{D}(f)$ is a symplectic map that preserves the subspace $\mathfrak{D}(U)$.

Proof. Clearly $\mathfrak{D}(U)$ is a subspace of $\mathfrak{D}(V)$, what remains to be shown is that $\mathfrak{D}(U)$ is isotropic. With $u, v, u', v' \in U$ we have generic elements of $\mathfrak{D}(U)$ given by $u \oplus \Omega_0(v, _)$ and $u' \oplus \Omega_0(v', _)$. The symplectic pairing evaluated on these two elements is

$$\begin{aligned} & \Omega(u \oplus \Omega_0(v, _), u' \oplus \Omega_0(v', _)) \\ &= \Omega_0(v', u) - \Omega_0(v, u') \\ &= 0 - 0 = 0 \end{aligned}$$

and so $\mathfrak{D}(U)$ is isotropic. Next, the action $\mathfrak{D}(f) : u \oplus \Omega_0(v, _) \mapsto f(u) \oplus \Omega_0(f^{-1}(v), _) \in \mathfrak{D}(U)$ and so $\mathfrak{D}(f)$ preserves the subspace $\mathfrak{D}(U)$ when f preserves the subspace U . \square

Given a $m \times 2n$ check matrix $\mathcal{H} = (\mathcal{H}_X \ \mathcal{H}_Z)$ the *doubled* check matrix $\mathfrak{D}(\mathcal{H})$ is a $2m \times 4n$ check matrix

$$\mathfrak{D}(\mathcal{H}) := \begin{pmatrix} \mathcal{H}_X & \mathcal{H}_Z & 0 & 0 \\ 0 & 0 & \mathcal{H}_Z & \mathcal{H}_X \end{pmatrix}. \quad (3)$$

By direct calculation we verify this is the check matrix for a quantum code (isotropic subspace), as promised by the functoriality lemma:

$$\mathfrak{D}(\mathcal{H})\Omega_{2n}\mathfrak{D}(\mathcal{H})^\top = \begin{pmatrix} 0 & \mathcal{H}\Omega_n\mathcal{H}^\top \\ \mathcal{H}\Omega_n\mathcal{H}^\top & 0 \end{pmatrix} = 0. \quad (4)$$

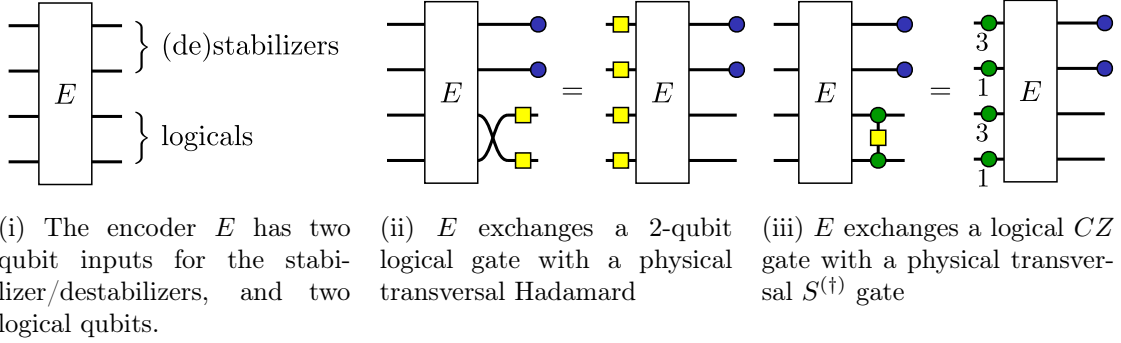


Figure 6: We show an encoding unitary E for the $[[4, 2, 2]]$ code as a circuit diagram, which flows in the algebraic direction, from right to left.

Theorem 3.2. Given a quantum code C with parameters $[[n, k, d]]$, we have $\mathfrak{D}(C)$ a CSS quantum code with parameters $[[2n, 2k, \geq d]]$.

Proof. By the functoriality lemma 3.1, we see that $\mathfrak{D}(C)$ is a $2n$ qubit quantum code. A check matrix for the codespace $\mathfrak{D}(C) = C \oplus \Omega_n(C, _)$ is given by (3), which has CSS form. Next, we examine logical operators $v \in \mathfrak{D}(C)^\perp$. Both v_X and $\Omega_n v_Z$ are in C^\perp , and $w(v) \geq w(v_X) + w(v_Z)$, which is lower bounded by d because one or both of $v_X, \Omega_n v_Z$ are not in C . \square

A closely related result is the following fault-tolerant property of fiber transversal Clifford gates.

Theorem 3.3. Given a quantum code C with parameters $[[n, k, d]]$ a logical Clifford on $\mathfrak{D}(C)$ that acts on each fiber separately is fault-tolerant up to distance d .

Proof. This is very similar to the proof of Theorem 3.2. See Appendix A. \square

Claim 3.4. A quantum code C is a CSS code iff $\mathfrak{D}(C) = C \oplus H(C)$.

We now give two operational characterizations of the CSS codes that are the double of some other code. The first characterization relies on the following definition. Given an n qubit CSS code $C = C_X \oplus C_Z$, a ZX -duality on C is a permutation $\tau : n \rightarrow n$ such that $\tau(C_X) = C_Z, \tau(C_Z) = C_X$ where the action of τ on subspaces of \mathbb{F}_2^n is by permuting coordinates.² The second characterization is in terms of concatenation with a CSS code with stabilizers $XXXX, ZZZZ$, logicals $XXII, ZIZI, XIXI, ZZII$. We call this *the* $[[4, 2, 2]]$ code, even though there are other CSS codes with these parameters.

Theorem 3.5. Given a CSS code C on $2n$ qubits, the following are equivalent:

- (1) C has a fixed-point-free involutory ZX -duality,
- (2) $C = \mathfrak{D}(C')$ for some n qubit quantum code C' , and
- (3) there is a concatenation of C with n copies of the $[[4, 2, 2]]$ code that is self-dual.

Proof. (1) \Rightarrow (2) Let $\tau : 2n \rightarrow 2n$ be a fixed-point-free involutory ZX -duality on C . This means that the orbits of τ have size two. Without loss of generality we can assume these

²This is slightly more general than the definition in [8].

orbits are of the form $\{i, i + n\}_{i=1, \dots, n}$. Let the check matrix for C be given by the $2m \times 4n$ matrix

$$\mathcal{H} = \begin{pmatrix} \mathcal{H}_X & 0 \\ 0 & \mathcal{H}_Z \end{pmatrix}$$

We see that $\tau H_Z^\top = H_X^\top A$ where A is an invertible $m \times m$ matrix. Therefore, we have

$$\begin{pmatrix} A^\top \mathcal{H}_X & 0 \\ 0 & \mathcal{H}_Z \end{pmatrix}$$

is in the form of a doubled check matrix (3).

(2) \Rightarrow (1) The converse direction follows because a doubled check matrix always has the above τ a (fixed-point-free involutory) ZX -duality.

(1) \Leftrightarrow (3) Concatenation corresponds to composing encoding circuits. The two qubit orbits of τ correspond to the pairs along which we concatenate with the $[[4, 2, 2]]$ code. The $[[4, 2, 2]]$ encoder satisfies the identity implementing a ZX -duality. See Fig. 6ii. \square

A stronger statement can be made: there is a bijection between CSS codes C with fixed-point-free involutory ZX -duality τ , and codes C' such that $C \cong \mathfrak{D}(C')$. In other words, there can be distinct codes C' and C'' that double to isomorphic codes $\mathfrak{D}(C') \cong \mathfrak{D}(C'')$. We will see an example of this in §5.2 and Fig. 12.

Given any of the conditions in Theorem 3.5 together with a condition on the X -type stabilizers, we have from [8] Theorem 7, that C will have a transversal CZ gate. Condition (3) is a generalization of the well-known construction of the $\{4, 8, 8\}$ colour code by concatenating the $[[4, 2, 2]]$ code with two copies of a toric code paired along a ZX -duality [15]. We write this concatenation along a ZX -duality τ as $[[4, 2, 2]] \otimes_\tau C$.

Claim 3.6. Given a quantum code C on n qubits the following are equivalent:

- (1) $\mathfrak{D}(C)$ has a fiber transversal CZ gate
- (2) C has a basis $\{v_i\}$ such that the parity of Y 's in each v_i is even
- (3) $[[4, 2, 2]] \otimes_\tau \mathfrak{D}(C)$ has a transversal $S^{(\dagger)}$ gate.

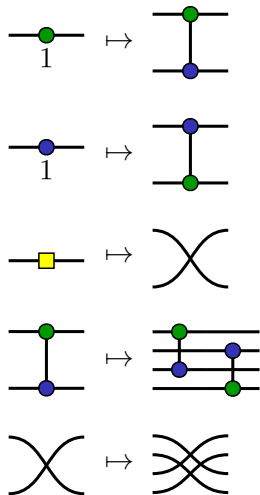
3.1 Lifting Cliffords

Recall that Cliffords in the phase-free ZX -calculus are generated by CX gates [25]. The next theorem is a consequence of the functoriality of $\mathfrak{D}(\cdot)$.

Theorem 3.7. The injective group homomorphism $\mathfrak{D} : \text{Sp}(2n, \mathbb{F}_2) \rightarrow \text{Sp}(4n, \mathbb{F}_2)$ lifts to a homomorphism $\mathfrak{D}' : \text{Sp}(2n, \mathbb{F}_2) \rightarrow \text{Cliff}(2n)$ whose image is given by Clifford unitary gates in the phase-free ZX -calculus with fixed-point-free involutory ZX -duality:

$$\begin{array}{ccc} & & \text{Cliff}(2n) \\ & \nearrow \mathfrak{D}' & \downarrow \\ \text{Sp}(2n, \mathbb{F}_2) & \xrightarrow{\mathfrak{D}} & \text{Sp}(4n, \mathbb{F}_2) \end{array}$$

Proof. We define \mathfrak{D}' on the generators (redundantly) as



Note we are using the “little-endian” symplectic convention for the string diagrams on the right-hand-side. This gives a (unitary) permutation representation of $\mathrm{Sp}(2n, \mathbb{F}_2)$ in the computational basis. It is straightforward to check that this agrees with the application of (1) to symplectic matrices M on $\mathbb{F}_2^n \oplus \mathbb{F}_2^n$:

$$\mathfrak{D}(M) = M \oplus (M^{-1})^\top.$$

□

For example, given a code C satisfying any of the conditions of Theorem 3.5, so that $C = \mathfrak{D}(C')$ a Hadamard on qubit i in the base code C' is lifted under \mathfrak{D}' to swapping the qubits in C in the fiber over i . We will explore further examples in §5 below.

This map \mathfrak{D}' also appears in the proof of Theorem 3.8 in [1], there denoted as $\llbracket \rrbracket^\natural$.

Claim 3.8. The Tanner graph of any symplectic matrix $M \in \mathrm{Sp}(2n, \mathbb{F}_2)$ gives a ZX-calculus diagram for $\mathfrak{D}'(M)$.

See Fig. 7 for the single qubit symplectic matrices $\mathrm{Sp}(2, \mathbb{F}_2)$ and the corresponding ZX-calculus diagrams.

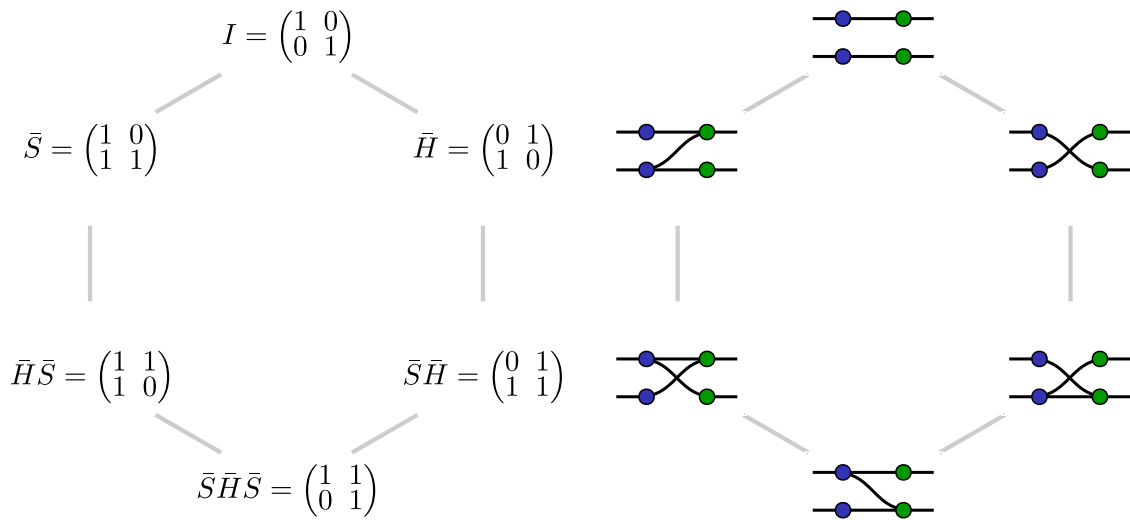
4 Genon codes

In this section we develop the theory of genon codes. Examples are discussed below in §5.

4.1 Genon graphs and genon codes

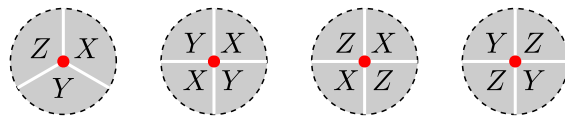
We are given a compact oriented surface S with a finite graph Γ embedded therein. This subdivides the surface into *faces*, *edges*, and *vertices*. Vertices are required to have valence three or four. Faces must have at least two edges, so that bigon faces are allowed, but monogon faces are not. We call such a Γ a *genon graph*.

A *genon code* on a genon graph Γ is a quantum code C where qubits are placed at vertices, stabilizers are placed on faces with the following allowed configurations at each vertex:



(i) Symplectic matrices for the local Clifford group on one qubit (ii) The corresponding Tanner graph of the Symplectic matrices

Figure 7: The Tanner graph for symplectic matrices in $\text{Sp}(2, \mathbb{F}_2)$ gives the ZX -calculus diagram for the lifted Clifford gate under \mathcal{D}' .

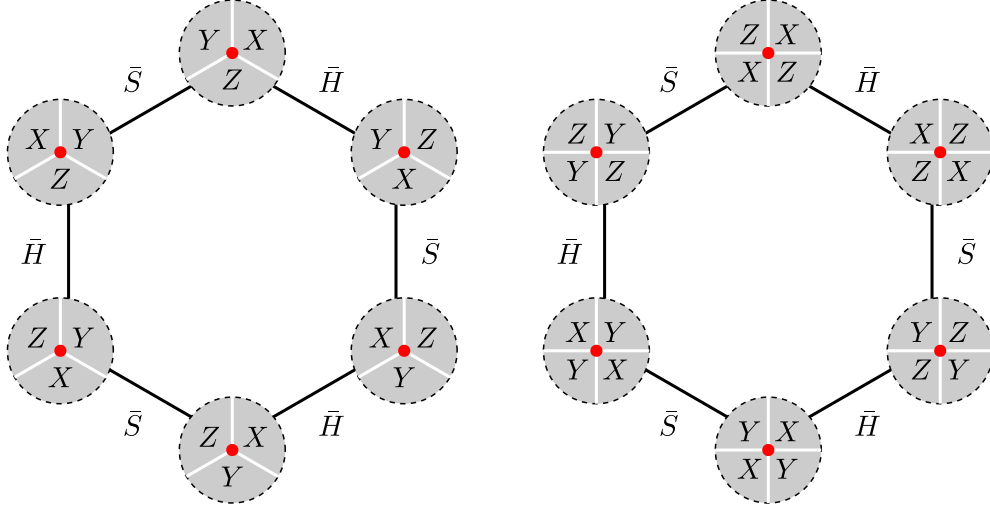


We will write (C, Γ) for a genon code C on Γ .

Theorem 4.1. Given a genon graph Γ with n vertices, there are $6n$ genon codes on Γ and they are all equivalent under local Clifford operations.

Proof. The local Clifford group acts transitively on the set of genon codes on Γ because any vertex configuration of valence $r = 3, 4$ is local Clifford equivalent to any other vertex configuration of valence r . Conversely, given a genon code, the stabilizer subgroup of the local Clifford group is trivial and so we have the result that there are $6n$ such distinct genon codes on a given graph Γ with n vertices. \square

It's worthwhile staring at an illustration of this proof to see how the local Clifford group acts on the 3-valent and 4-valent vertices. You really do get 6 different configurations at each vertex, and the local Clifford group moves between all of these:



Lemma 4.2. Let C be a genon code on Γ encoding k logical qubits. If Γ is bicolourable then $k = V - F + 2$, otherwise $k = V - F + 1$.

Proof. For any stabilizer code with n qubits and check matrix \mathcal{H} we have that $k = n - \text{rank}(\mathcal{H}) = V - \text{rank}(\mathcal{H})$. For a genon code C on Γ , \mathcal{H} is given by stabilizers living on the faces. Let Γ be bicolourable, with faces either black or white. Then Γ has only four valent vertices, and we get a linear dependent combination of white stabilizers, and also for black stabilizers. Conversely, any linear dependent combination of stabilizers is a sum of either of the black or white faces. Therefore, $k = V - F + 2$, and moreover, this argument runs backwards so that $k = V - F + 2$ implies bicolourable faces. A similar argument shows that a lack of bicolourable faces is equivalent to $k = V - F + 1$. In this case the one linear dependency comes from the combination of all the face stabilizers. \square

Theorem 4.3. Let C be a genon code on Γ encoding k logical qubits, with m the number of 3-valent vertices, and g the genus of Γ . If Γ is bicolourable then $k = 2g$ and $m = 0$, otherwise $k = 2g + \frac{m}{2} - 1$.

Proof. Let V_3 be the number of 3-valent vertices, and V_4 be the number of 4-valent vertices. Then we see the number of edges is $E = \frac{3}{2}V_3 + 2V_4$. Writing the Euler characteristic:

$$\begin{aligned} \chi &= 2 - 2g = V - E + F \\ &= V_3 + V_4 - \frac{3}{2}V_3 - 2V_4 + F \\ &= F - \frac{1}{2}V_3 - V_4. \end{aligned}$$

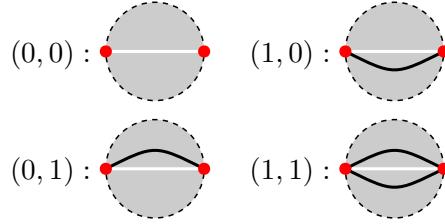
If Γ is bicolourable, then $V_3 = 0$ and by the previous lemma we find $k = V_4 - F + 2$. Substituting $F = 2 + V_4 - k$ into the above equation for χ we get $2 - 2g = 2 + V_4 - k - V_4$ and so $k = 2g$. If Γ is not bicolourable the previous lemma gives $F = V_3 + V_4 + 1 - k$ and so $2 - 2g = V_3 + V_4 + 1 - k - \frac{1}{2}V_3 - V_4$ which gives $k = 2g + \frac{m}{2} - 1$ as required. \square

4.2 String operators

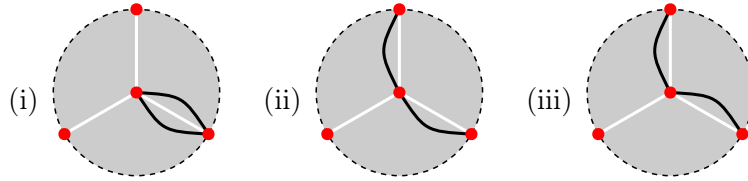
See SY [33] §4 and GS [19] §III D.

We'd like to refer to logical operators of a genon code up to local Clifford equivalence. This is a theory of *string operators* based only on the graph Γ . This will be a classical binary code S , which is then linearly mapped onto the logical space C^\perp of a given genon code C on Γ .

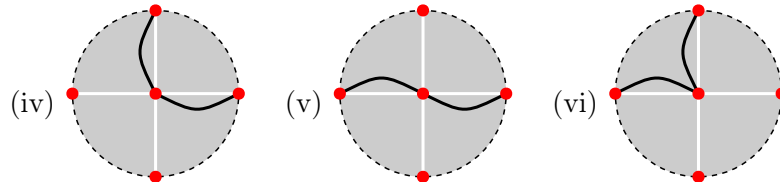
Given a genon graph Γ we associate a vector space \mathbb{F}_2^{2E} whose basis is the edge-face pairs of Γ . In other words, every edge has a vector space \mathbb{F}_2^2 associated. We notate the four vectors in this space with black lines



and similarly for vectors in \mathbb{F}_2^E . We now define the subspace $S \subset \mathbb{F}_2^{2E}$ of *string operators*, by considering the allowed string operators around the 3-valent vertices and 4-valent vertices. Around 3-valent vertices, we have a vector space \mathbb{F}_2^6 , whose intersection with S is a 5-dimensional space spanned by



and rotations/reflections. These give all even parity vectors of \mathbb{F}_2^6 . Around the 4-valent vertices we have a vector space \mathbb{F}_2^8 , whose intersection with S is a 6-dimensional space spanned by

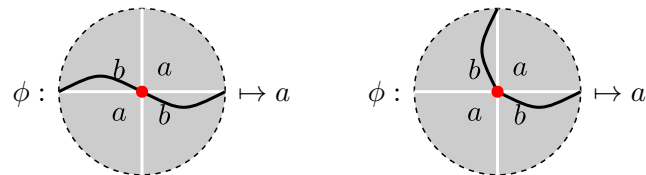


and rotations/reflections. Note these diagrams are not all linearly independent, for example (i)+(ii)=(iii) and (iv)+(v)=(vi).

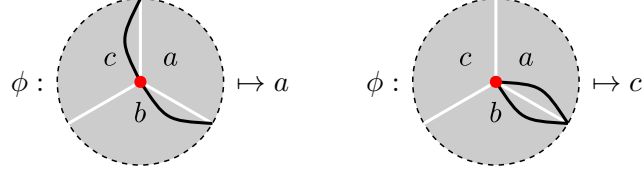
Given a genon code C on Γ we define a linear map of string operators to logical operators

$$\phi : S \rightarrow C^\perp$$

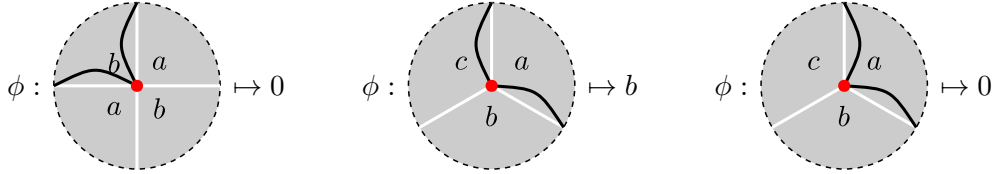
on basis elements of S as follows. At a 4-valent vertex:



and rotations/reflections. At a 3-valent vertex:

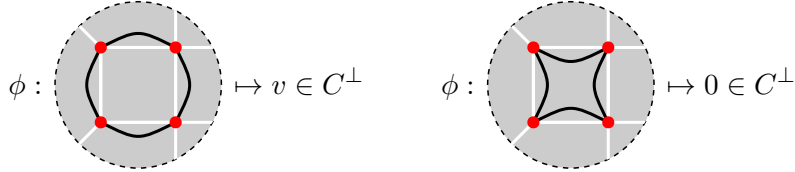


and rotations/reflections. For example, linearity of ϕ implies the following:



Notice that the kernel of ϕ is non-trivial, in other words there is some redundancy in these string operators.

Using ϕ we can pick out a stabilizer generator $v \in C^\perp$ with a string operator *external* to the corresponding face, however the string operator *internal* to a face is sent to zero, for example:



We summarize this in the following theorem.

Theorem 4.4. Given a genon code C with parameters $[[n, k, d]]$, on a graph Γ we have that

$$\dim(S) = \begin{cases} 2k + 2F - 2 & \text{if } \Gamma \text{ is bicolourable} \\ 2k + 2F - 1 & \text{otherwise} \end{cases} = \begin{cases} 2n + 2 & \text{if } \Gamma \text{ is bicolourable} \\ 2n + 1 & \text{otherwise} \end{cases}$$

and $\phi : S \rightarrow C^\perp$ is surjective with kernel spanned by the internal face string operators.

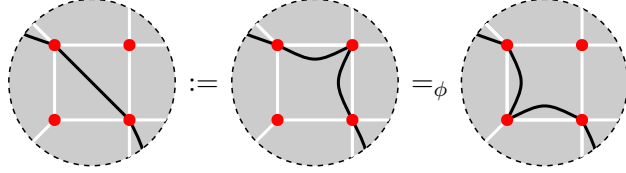
Proof. Given a logical operator $v \in C^\perp$ we can construct a string operator in $u \in S$ locally such that $\phi(u) = v$. This is done by cases. To find the kernel of ϕ we see that all the internal face string operators are linearly independent, there are F many of these, where F is the number of faces of Γ and

$$F = \begin{cases} n - k + 2 & \text{if } \Gamma \text{ is bicolourable} \\ n - k + 1 & \text{otherwise} \end{cases}$$

□

This theorem makes intuitive sense from the homological point of view: stabilizer generators are given by operators that bound a region, so they have an inside. Loosely speaking, the extra information found in the string operators S includes inside-out stabilizers, which ϕ must send to zero.

Because the internal face string operators are sent to zero by ϕ we define the diagrammatic shorthand, or syntactic sugar:

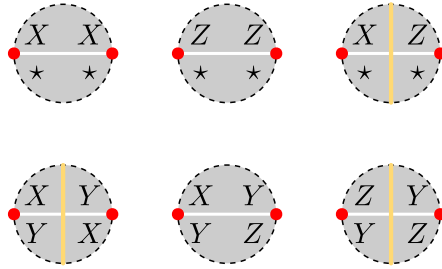


where the ϕ subscript refers to equality in the image of ϕ . In words, string operators can pass directly across faces and don't need to wind around the inside. Examples of the use of this string diagram calculus are given in Fig. 11.

4.3 Domain walls

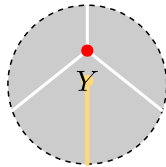
Given a genon code C on a graph Γ , we define a unique decoration on Γ , called the *domain walls* as follows:

(1) Every edge lies between two faces and we place domain walls between the center of the two faces according to the rules:



where the star \star denotes any Pauli consistent with the genon code rules. For example a YY configuration along one side of an edge is covered by these rules because on the other side of the edge will be XX , ZZ or XZ .

(2) Each face with a Y at a trivalent vertex has a domain wall from the center of the face to the Y operator (the face-vertex flag):



Theorem 4.5. At the center of each face there is an even number of domain walls coming together.

Proof. Given a genon code C we call the parity of a face to be the number domain walls incident at the center mod 2. Step 1: we see that local Clifford operators preserve the domain wall parity at each face. This is done by cases. Step 2: for each face, use local Clifford operators to convert this face stabilizer into a pure X type stabilizer. This has zero domain walls, which is even parity. \square

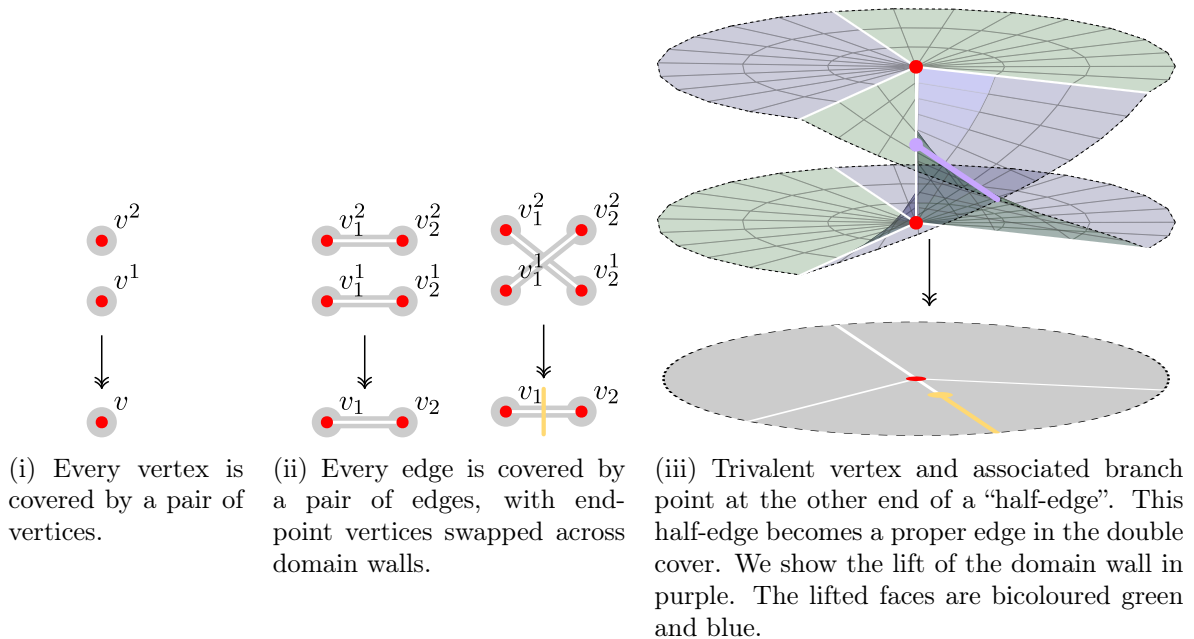


Figure 8: The double cover of a genon graph Γ relative to a code C is constructed dimension wise, starting with vertices, then edges, then faces.

From this theorem we see that if a domain wall has an endpoint it will be at the Y operator of a 3-valent vertex (and never at the center of a face). We call these termination points *genons*.

Given a genon code C we see that there is one way to decorate the surface Γ with domain walls, however the converse is not true.

4.4 Double covers of genon codes

Given a genon code C on a graph Γ , we define the *double cover* of Γ relative to C written $\mathfrak{D}(\Gamma, C)$, as follows:

(Dimension 0) Every vertex $v \in \Gamma$ is covered by two vertices in $\mathfrak{D}(\Gamma, C)$, called the *fiber* over v . This fiber is ordered, and we write the two vertices over v as v^1 and v^2 . See Fig. 8i.

(Dimension 1) Every edge $e \in \Gamma$, with vertices v_1, v_2 , is covered by two edges in $\mathfrak{D}(\Gamma, C)$, called the *fiber* over e , written e^1 and e^2 . If e does not cross a domain wall then e^1 has vertices v_1^1, v_2^1 , and e^2 has vertices v_1^2, v_2^2 . If e does cross a domain wall then e^1 has vertices v_1^1, v_2^2 , and e^2 has vertices v_1^2, v_2^1 . See Fig. 8ii.

(Genons) Every 3-valent vertex $v \in \Gamma$, with incident face $f \in \Gamma$ whose stabilizer in C supports a Y operator is covered by a single edge in $\mathfrak{D}(\Gamma, C)$ with vertices v^1, v^2 .

(Dimension 2) Each face in $\mathfrak{D}(\Gamma, C)$ is constructed by lifting closed paths γ around the edges of a face $f \in \Gamma$. The lifted edges in these lifted paths then form the edges of a face. When the path γ encounters a genon at v , the edge between v^1, v^2 is included in the lifted face, see Fig. 8iii. If the parity of the domain walls around f is even there will be two lifted faces f^1, f^2 , coming from two possible lifts of γ , otherwise there is only one lifted face f^1 which comes from the unique lift of γ .

Given a genon code C on Γ we say that C is *clean* when the stabilizers around 4-valent

vertices support only X -type and Z -type operators. In this sense, there are no unnecessary Y operators.

Claim 4.6. Given a clean genon code C on Γ , then $\mathfrak{D}(C)$ is a CSS genon code on $\mathfrak{D}(\Gamma, C)$.

Claim 4.7. Given a clean genon code C on Γ , then $\mathfrak{D}(\Gamma, C)$ is bicolourable and supports two CSS genon codes, one of which is $\mathfrak{D}(C)$ and the other its dual.

Claim 4.8. Given a genon code C on Γ , with parameters $[[n, k, d]]$ then $[[4, 2, 2]] \otimes_{\tau} \mathfrak{D}(C)$ is a self-dual $[[4n, 2k, \geq d]]$ code.

Claim 4.9. Given a genon code C on Γ , then Γ is bicolourable iff $[[4, 2, 2]] \otimes_{\tau} \mathfrak{D}(C)$ is a colour code.

5 Example genon codes and protocols

5.1 Genus zero

For this example, the genon graph Γ is a tetrahedron inscribed on a sphere: there are four qubits and four face stabilizers, see Fig. 9. A nice choice for C is given by the redundant stabilizer group generators:

$$\langle XYZI, IXYZ, ZIXY, YZIX \rangle.$$

Evidently, this code has a $\mathbb{Z}/4$ cyclic symmetry $1 \mapsto 2 \mapsto 3 \mapsto 4 \mapsto 1$, whose action on the logical operators

$$L_X = ZXII, \quad L_Z = IZXI$$

is a logical Hadamard gate:

$$\begin{aligned} L_X &\mapsto IZXI = L_Z \\ L_Z &\mapsto IIZX = L_X \cdot (ZIXY) \cdot (IXYZ). \end{aligned}$$

Moreover, it turns out we can perform any of the $4! = 24$ permutations on the physical qubits followed by local Clifford gates, and these yield all the single qubit logical Clifford gates for

this code. We tabulate the complete protocol:

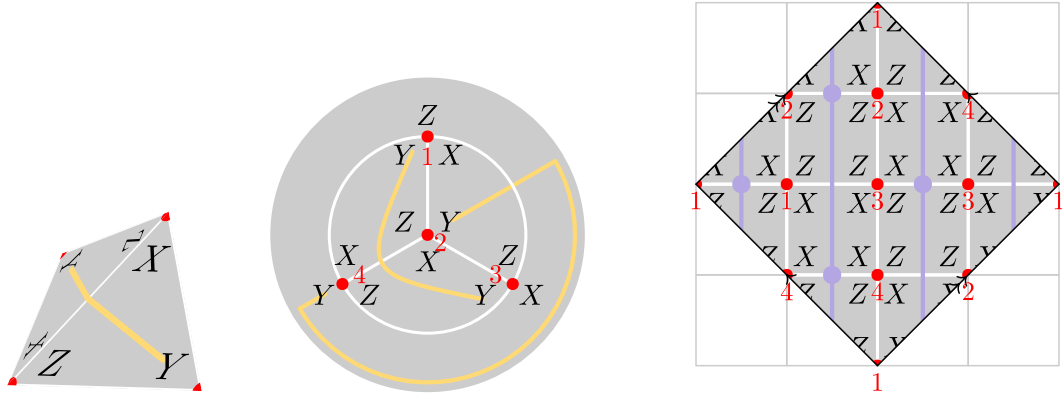
permutation	local Clifford gate	logical gate
(1, 2, 3, 4)	$IIII$	I
(1, 2, 4, 3)	$\bar{S}(\bar{H} \cdot \bar{S} \cdot \bar{H})(\bar{S} \cdot \bar{H})(\bar{H} \cdot \bar{S})$	$(\bar{H} \cdot \bar{S} \cdot \bar{H})$
(1, 3, 2, 4)	$(\bar{H} \cdot \bar{S} \cdot \bar{H})(\bar{S} \cdot \bar{H})(\bar{H} \cdot \bar{S})\bar{S}$	\bar{S}
(1, 3, 4, 2)	$(\bar{H} \cdot \bar{S})\bar{S}(\bar{H} \cdot \bar{S} \cdot \bar{H})(\bar{S} \cdot \bar{H})$	$(\bar{H} \cdot \bar{S})$
(1, 4, 2, 3)	$(\bar{S} \cdot \bar{H})(\bar{H} \cdot \bar{S})\bar{S}(\bar{H} \cdot \bar{S} \cdot \bar{H})$	$(\bar{S} \cdot \bar{H})$
(1, 4, 3, 2)	$\bar{H}\bar{H}\bar{H}\bar{H}$	\bar{H}
(2, 1, 3, 4)	$(\bar{S} \cdot \bar{H})(\bar{H} \cdot \bar{S})\bar{S}(\bar{H} \cdot \bar{S} \cdot \bar{H})$	$(\bar{H} \cdot \bar{S} \cdot \bar{H})$
(2, 1, 4, 3)	$\bar{H}\bar{H}\bar{H}\bar{H}$	I
(2, 3, 1, 4)	$\bar{S}(\bar{H} \cdot \bar{S} \cdot \bar{H})(\bar{S} \cdot \bar{H})(\bar{H} \cdot \bar{S})$	$(\bar{S} \cdot \bar{H})$
(2, 3, 4, 1)	$IIII$	\bar{H}
(2, 4, 1, 3)	$(\bar{H} \cdot \bar{S})\bar{S}(\bar{H} \cdot \bar{S} \cdot \bar{H})(\bar{S} \cdot \bar{H})$	\bar{S}
(2, 4, 3, 1)	$(\bar{H} \cdot \bar{S} \cdot \bar{H})(\bar{S} \cdot \bar{H})(\bar{H} \cdot \bar{S})\bar{S}$	$(\bar{H} \cdot \bar{S})$
(3, 1, 2, 4)	$(\bar{H} \cdot \bar{S})\bar{S}(\bar{H} \cdot \bar{S} \cdot \bar{H})(\bar{S} \cdot \bar{H})$	$(\bar{H} \cdot \bar{S})$
(3, 1, 4, 2)	$(\bar{H} \cdot \bar{S} \cdot \bar{H})(\bar{S} \cdot \bar{H})(\bar{H} \cdot \bar{S})\bar{S}$	\bar{S}
(3, 2, 1, 4)	$\bar{H}\bar{H}\bar{H}\bar{H}$	\bar{H}
(3, 2, 4, 1)	$(\bar{S} \cdot \bar{H})(\bar{H} \cdot \bar{S})\bar{S}(\bar{H} \cdot \bar{S} \cdot \bar{H})$	$(\bar{S} \cdot \bar{H})$
(3, 4, 1, 2)	$IIII$	I
(3, 4, 2, 1)	$\bar{S}(\bar{H} \cdot \bar{S} \cdot \bar{H})(\bar{S} \cdot \bar{H})(\bar{H} \cdot \bar{S})$	$(\bar{H} \cdot \bar{S} \cdot \bar{H})$
(4, 1, 2, 3)	$IIII$	\bar{H}
(4, 1, 3, 2)	$\bar{S}(\bar{H} \cdot \bar{S} \cdot \bar{H})(\bar{S} \cdot \bar{H})(\bar{H} \cdot \bar{S})$	$(\bar{S} \cdot \bar{H})$
(4, 2, 1, 3)	$(\bar{H} \cdot \bar{S} \cdot \bar{H})(\bar{S} \cdot \bar{H})(\bar{H} \cdot \bar{S})\bar{S}$	$(\bar{H} \cdot \bar{S})$
(4, 2, 3, 1)	$(\bar{H} \cdot \bar{S})\bar{S}(\bar{H} \cdot \bar{S} \cdot \bar{H})(\bar{S} \cdot \bar{H})$	\bar{S}
(4, 3, 1, 2)	$(\bar{S} \cdot \bar{H})(\bar{H} \cdot \bar{S})\bar{S}(\bar{H} \cdot \bar{S} \cdot \bar{H})$	$(\bar{H} \cdot \bar{S} \cdot \bar{H})$
(4, 3, 2, 1)	$\bar{H}\bar{H}\bar{H}\bar{H}$	I

Using this protocol we can lift all of these gates to logical Clifford gates on the $[[8, 2, 2]]$ code by Theorem 3.7. We see the (1, 4, 3, 2) permutation for logical \bar{H} and the (1, 3, 2, 4) for logical \bar{S} , as well as (2, 1, 4, 3) and (3, 4, 1, 2) for logical I , agree with the anyon calculations in §2.1.1. The two logical gates \bar{H}, \bar{S} generate the whole single qubit Clifford group and will be used in the experiments §6 below. We also note this $[[4, 1, 2]]$ code is local Clifford equivalent to the $[[4, 1, 2]]$ triangular colour code presented in [24], §5.2.

The surface codes, such as the $[[5, 1, 2]]$ code are genon codes on a sphere, Fig. 10 (i). The missing external stabilizer forms the back of the sphere, and contains the domain walls. In general, any surface code with a single boundary component forms a genon code in this way.

As a next example we take Landahl's jaunty code [26]. This is a $[[14, 3, 3]]$ code on a rhombic dodecahedron inscribed on a sphere, Fig. 10(iv).

Below we tabulate some of these examples and their symplectic doubles.



(i) We take a genus graph to be a tetrahedron inscribed on a sphere. (ii) The same graph with one face splayed out to infinity. Qubits are numbered in red 1-4. (iii) The double cover, with qubits numbered as to which qubit is covered in the base $[[4, 1, 2]]$ code. The covering branch points (4 of them) and domain walls are shown in purple.

Figure 9: A genus zero $[[4, 1, 2]]$ code is double covered by an $[[8, 2, 2]]$ toric code.

base code	genons	see Fig.	symplectic double	genus
$[[4, 1, 2]]$	$m = 4$	9	$[[8, 2, 2]]$	$g = 1$
$[[5, 1, 2]]$	$m = 4$	10 (i)&(ii)	$[[10, 2, 3]]$	$g = 1$
$[[6, 2, 2]]$	$m = 6$	10 (iii)	$[[12, 4, 2]]$	$g = 2$
$[[14, 3, 3]]$	$m = 8$	10 (iv)&(v)	$[[28, 6, 3]]$	$g = 3$

5.2 Genus one

We parameterize these by two integers (a, b) . We view these periodic lattices as quotients of the Gaussian integers: $\mathbb{Z}[i]/\langle a + bi \rangle$. See Fig. 11. The resulting code has parameters $[[n, k, d]]$ with

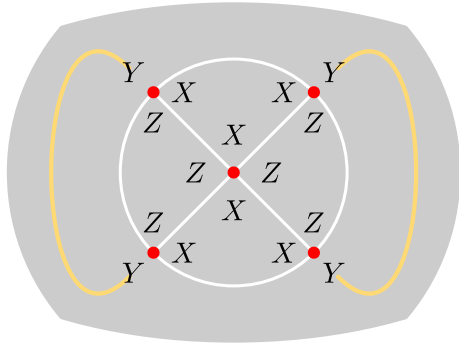
$$n = a^2 + b^2, \quad k = \begin{cases} 1 & \text{if } n \text{ odd} \\ 2 & \text{if } n \text{ even} \end{cases}, \quad d = \begin{cases} a + b & \text{if } n \text{ odd} \\ \max(a, b) & \text{if } n \text{ even} \end{cases}.$$

See [33], Theorem 3.9., where they define a family of codes called the cyclic toric codes when $\gcd(a, b) = 1$.

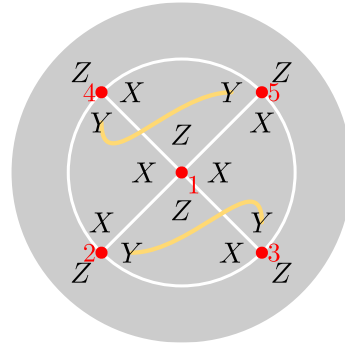
We make a table of some of these:

	$a = 0$	$a = 1$	$a = 2$	$a = 3$	$a = 4$	$a = 5$	$a = 6$	$a = 7$
$b = 2$	$[[4, 2, 2]]$	$[[5, 1, 3]]$	$[[8, 2, 2]]$					
$b = 3$	$[[9, 1, 3]]$	$[[10, 2, 3]]$	$[[13, 1, 5]]$	$[[18, 2, 3]]$				
$b = 4$	$[[16, 2, 4]]$	$[[17, 1, 5]]$	$[[20, 2, 4]]$	$[[25, 1, 7]]$	$[[32, 2, 4]]$			
$b = 5$	$[[25, 1, 5]]$	$[[26, 2, 5]]$	$[[29, 1, 7]]$	$[[34, 2, 5]]$	$[[41, 1, 9]]$	$[[50, 2, 5]]$		
$b = 6$	$[[36, 2, 6]]$	$[[37, 1, 7]]$	$[[40, 2, 6]]$	$[[45, 1, 9]]$	$[[52, 2, 6]]$	$[[61, 1, 11]]$	$[[72, 2, 6]]$	
$b = 7$	$[[49, 1, 7]]$	$[[50, 2, 7]]$	$[[53, 1, 9]]$	$[[58, 2, 7]]$	$[[65, 1, 11]]$	$[[74, 2, 7]]$	$[[85, 1, 13]]$	$[[98, 2, 7]]$

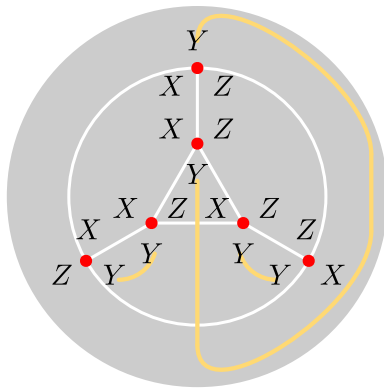
So far all these genus one codes have no genons. In Fig. 13 we show a $[[12, 4, 3]]$ genus one code with six genons.



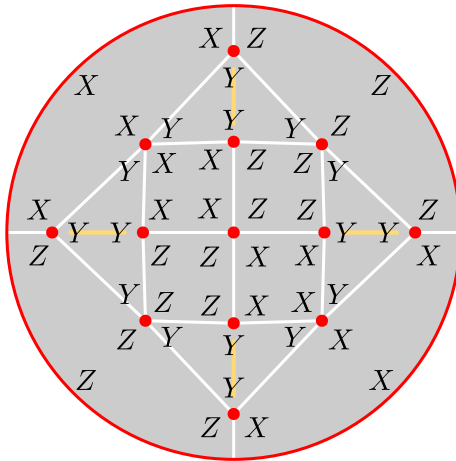
(i) This is the well-known $[[5, 1, 2]]$ surface code.



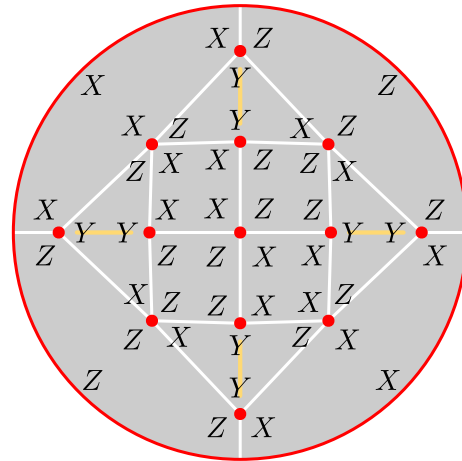
(ii) Another $[[5, 1, 2]]$ code on the same graph. This is a non-CSS code, local Clifford equivalent to (i).



(iii) This is a $[[6, 2, 2]]$ code. Qubits are placed on the vertices of a triangular prism. There are two triangular faces and three square faces.



(iv) Landahl's jaunty $[[14, 3, 3]]$ code We show this in splayed view with one qubit stretched out to infinity.



(v) A local Clifford equivalent $[[14, 3, 3]]$ is in a clean configuration which means the valence 4 vertices see only X and Z operators, and ensures the doubled code is a genon code, Thm.4.6.

Figure 10: Various genon codes that have genus zero.

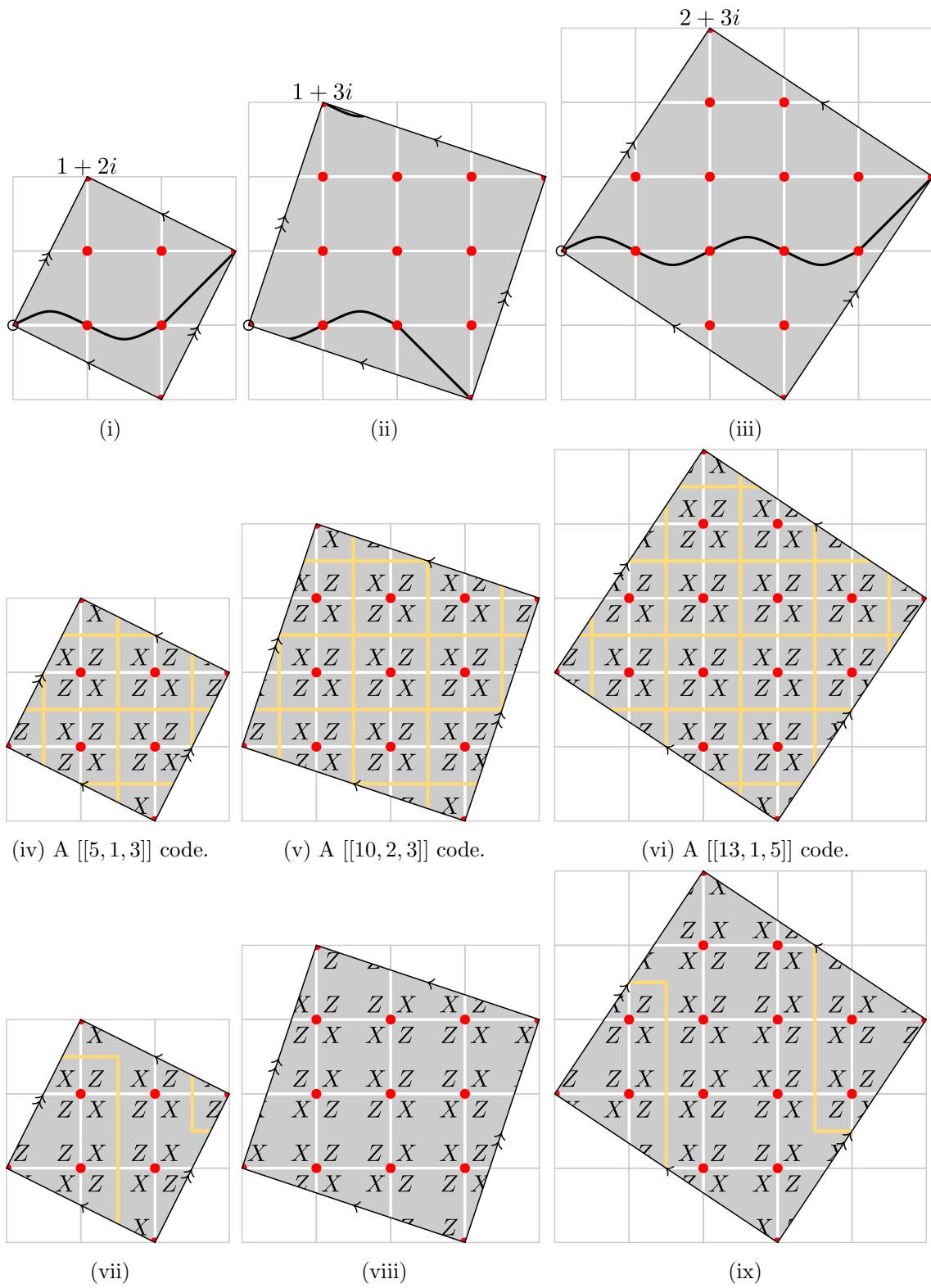
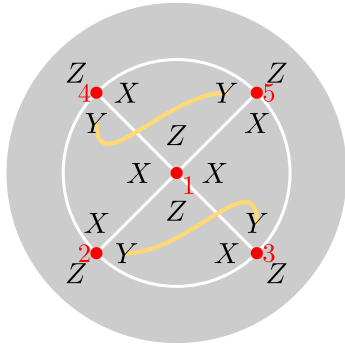
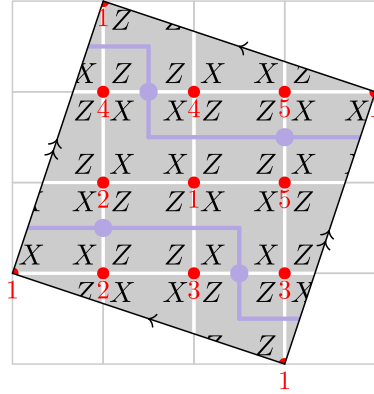


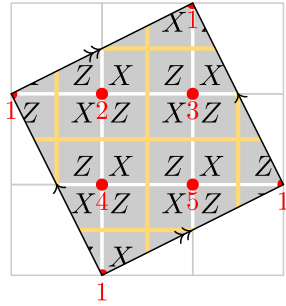
Figure 11: (i)-(iii): genon graphs built from quotients $\mathbb{Z}[i]/\langle a+bi \rangle$ and logical string operators. We marked the origin as well as the Gaussian integer $a+bi$. (iv)-(vi): the $XZZX$ code and corresponding domain walls. (vii)-(ix): local Clifford equivalence can remove (some) domain walls.



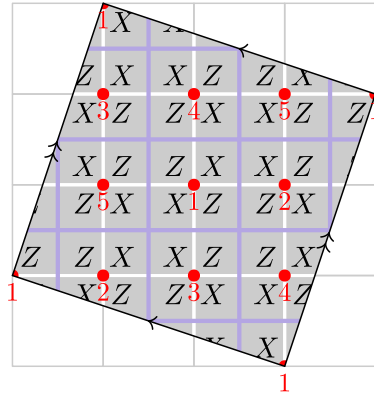
(i) The genus zero base code with parameters $[[5, 1, 2]]$



(ii) The $[[10, 2, 3]]$ double cover.



(iii) The genus one base code is the $[[5, 1, 3]]$ code.



(iv) The $[[10, 2, 3]]$ double cover.

Figure 12: On the $[[10, 2, 3]]$ code there is a total of six ZX -dualities satisfying the requirements of Theorem 3.5. Five of these correspond to genus zero base code, and the other is the genus one base code. Here we show an example of a genus zero base code (i) as covered by (ii), as well as a genus one code (iii) as covered by (iv). The qubits are enumerated in each base, and these numbers are lifted into the respective cover.

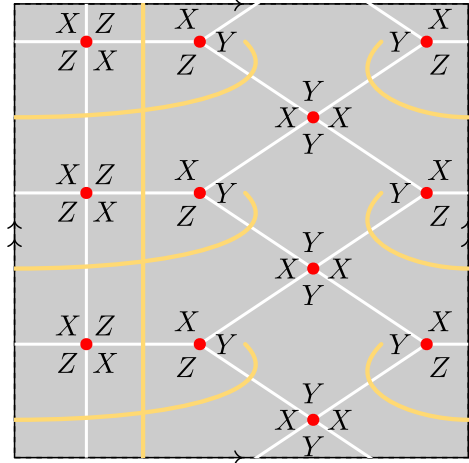


Figure 13: This genus one code has six genons and parameters $[[12, 4, 3]]$.

6 Experimental results

The permutations required for implementing genon protocols and fault-tolerant gates resulting from the lifting theorem, can be efficiently realized on a hardware with high-connectivity. In architectures with fixed qubit structures and thus restricted connectivity, qubit permutations are realized through circuit-level swapping, moving information between two separate qubits by performing a series of local swaps of adjacent qubits between them, thus increasing the overall circuit depth. In systems with arbitrary connectivity, qubit permutations can be realized through a simple "relabeling" of the physical qubits.

Quantinuum's trapped-ion H1-1 device is based the quantum CCD (QCCD) architecture [36, 32] realizes all-to-all connectivity by using ion-transport operations. Ions are able to physically move around the linear trap, physically swapping locations as needed. As such, the H1-1 realizes fault-tolerant genon protocols with little overhead, incurring only noise from transport as no circuit-level swapping is required.

The H1-1 device uses 20 $^{171}\text{Yb}^+$ ions for physical qubits and 20 $^{138}\text{Ba}^+$ ions for sympathetic cooling, totally to 40 physical ions in the trap. Gates are executed via stimulated Raman transitions implemented with off-resonant lasers directed in five distinct regions. During the course of these experiments, the average physical fidelities for the single-qubit and two-qubit gates, as measured by randomized benchmarking [30] experiments averaged over all five gate zones, were $3.2(5) \times 10^{-5}$ and $9.2(5) \times 10^{-4}$ respectively. State preparation and measurement errors were also measured to be $2.7(1) \times 10^{-3}$.

Idling and transport error are more difficult to more difficult to characterize in the QCCD architecture as different circuits require different transport sequences. Indeed, depending on the circuit, certain permutations may not require additional transport. This gives the opportunity but not a prior guarantee for the compiler to reduce transport costs to next to zero, potentially allowing for very low error rate over heads. But more work needs to be done to study transport overheads for these sort of logical gates in practice. We leave it to future work to characterize how such transport impacts the logical gate fidelity of the protocol realized. For further description of the H1-1 hardware benchmarks and specifications, see [32, 2].

In this work, we realized three different experimental implementations of the theory work

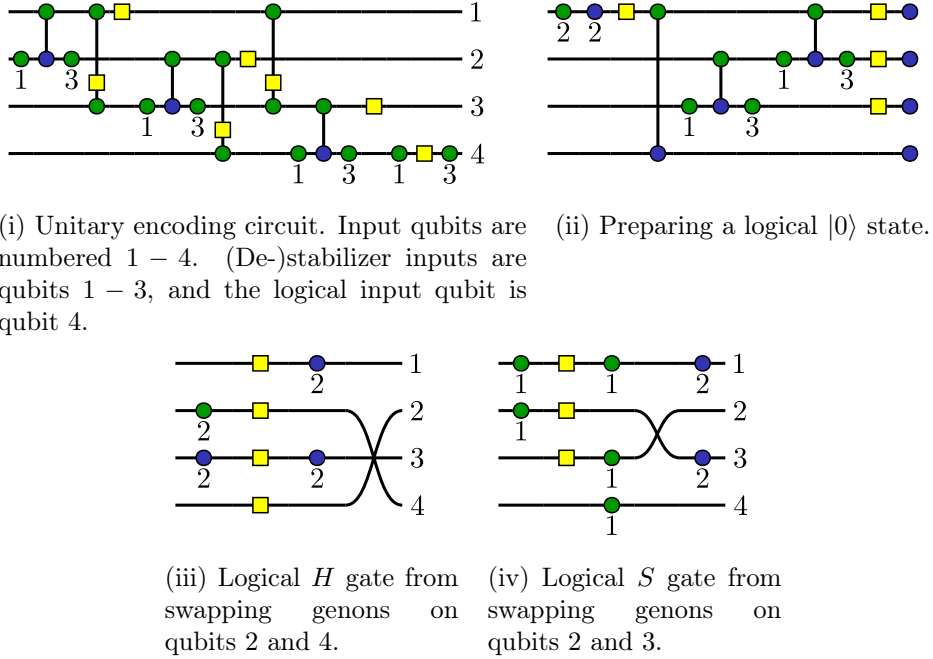


Figure 14: The $[[4,1,2]]$ protocol implementing single qubit Clifford gates by braiding (swapping) genons.

outlined above on the H1-1 QCCD device. First, we realized genon braiding in the $[[4, 1, 2]]$, done by performing local Cliffords and qubit permutations. Such permutations are physically realized through ion-transport. We demonstrate the ability to produce the full Clifford group through the demonstration of *logical* randomized benchmarking, thus showcasing the power of the genon braiding technique. Next, by lifting the logical S gate from the $[[4, 1, 2]]$ code, we benchmark a logical CX gate of the $[[8,2,2]]$ code, the double cover of the $[[4, 1, 2]]$. This logical gate, involving qubit permutations, again is efficiently realized through the qubit relabelling enabled by ion transport primitives. Finally, we realize another implementation two qubit logical gate from lifting the transversal SH gate on the $[[5, 1, 3]]$ code. We benchmark this gate in a similar manner to the CX on the $[[8, 2, 2]]$ but this time require proper decoding (rather than post-selection).

6.1 The $[[4,1,2]]$ protocol

As a demonstration of genon braiding, we ran *logical randomized benchmarking* [30, 14, 31], on the $[[4, 1, 2]]$ genon code using the circuits shown in Fig. 14. See Appendix B for example QASM. The protocol proceeds in 3 steps:

(Step 1) We begin by preparing the logical $|0\rangle$ state using the circuit in Fig. 14(ii).

(Step 2) We apply a random sequence of N logical Clifford gates. There are 192 Clifford gates, or 24 up to phase, to choose from. This group is generated by the H and S gates, which at the physical level is realized through concatenation of the circuits in Fig. 14(iii) and (iv). We also use the redundant Clifford generators X and Z , coming from the logical Pauli operators of the $[[4, 1, 2]]$ code. Each resulting concatenation is compiled for the H1-1 device into at most four single qubit Clifford gates; qubit permutations are implemented via

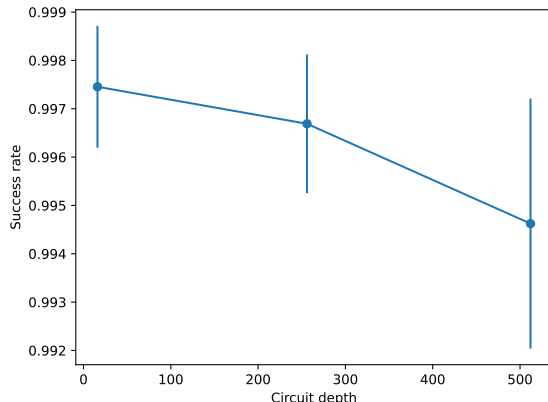


Figure 15: The survival probability from the randomized benchmarking protocol on the $[[4, 1, 2]]$ code, as realized on the H1-1 machine. Circuit depths 16 and 256 were ran with 1600 shots each and circuit depth 512 was ran with 800 shots. We note this graph seems to show a quadratic decay as opposed to the linear decay more commonly seen by randomized benchmarking.

relabelling.

(Step 3) We apply the inverse of the encoding circuit in Fig. 14(i). This gives syndrome qubits 1,2 and 3 and (unencoded) logical qubit 4. We apply the inverse of the Clifford operation in (Step 2) on the qubit 4, and then measure all qubits in the $\langle 0, 1 |$ basis.

We treat this as an *error detecting* code, so the result of the measurement is discarded if any of the syndrome bits are non-zero. Otherwise we record *survival* if the logical bit is zero. We ran three different random sequences of lengths $N = 16$, 256 and 512. Using Step 1-3 above we sample 16 circuits for each of $N = 16$ and $N = 256$, and for $N = 512$ we sampled 8 circuits. Each circuit is then executed for 100 shots. The discard counts were 28/1600, 90/1600, and 56/800 respectively. The survival probability is plotted in Fig. 15.

In general, it can be hard to extract the logical fidelity from the randomized benchmarking protocol without interleaving QEC cycles [31]. From the randomized benchmarking protocol, we would expect to see a linear decay in the survival probability resulting from accumulation of errors [30]. However, we observe that the curve seen in Fig. 15, matches a quadratic fit instead of a linear one. Further investigation is needed to conclude whether such a logical randomized benchmarking experiment, without interleaving QEC cycles, is sufficient to extract a reliable logical error rate and is outside the scope of this work. Here we use the randomize benchmarking protocol as a proof of practice that genon braiding on the $[[4, 1, 2]]$ can be used to realize the full Clifford group and easily implemented on the H1-1 device.

6.2 The $[[8, 2, 2]]$ protocol

In this experiment we benchmark a logical CX gate on the $[[8, 2, 2]]$ toric code. This code is the double cover of the $[[4, 1, 2]]$ base code, and the logical CX is the lift of the logical S gate on the base code given in Fig. 14 (iv), using Theorem 3.7. The fibers over the base qubits 1, 2, 3, 4 are $\{1, 5\}$, $\{2, 6\}$, $\{3, 7\}$, $\{4, 8\}$ respectively, see Fig. 16.

To benchmark this CX gate we run $4 + 8 = 12$ circuits comprised of the following:

logical operation	logical state	experimental errors	simulated errors	logical operation	logical state	experimental errors	simulated errors
I	$ 00\rangle$	3	4.8	I	$ ++\rangle$	0	0.5
I	$ 11\rangle$	4	6.9	I	$ --\rangle$	0	0.6
$CX_{1,0}$	$ 00\rangle$	0	4.3	$CX_{1,0}$	$ ++\rangle$	0	0.7
$CX_{1,0}$	$ 01\rangle$	2	4.7	$CX_{1,0}$	$ +-\rangle$	0	0.5
$CX_{1,0}$	$ 10\rangle$	2	3.6	$CX_{1,0}$	$ -+\rangle$	0	0.3
$CX_{1,0}$	$ 11\rangle$	3	4.6	$CX_{1,0}$	$ --\rangle$	0	1.0

Table 1: The number of logical errors found for the $[[8, 2, 2]]$ code simulations and experiments. Here the logical operation I is meant to imply the state preparation and measurement errors seen while preparing the individual two-qubit logical states. A series of experiments were also performed implementing the logical CX gate between the two logical qubits contained in the $[[8, 2, 2]]$ code block.

- State preparation and measurement (SPAM) circuits, for each of logical $|00\rangle$, $|11\rangle$, $|++\rangle$, and $|--\rangle$.
- The action of the logical CX on the two qubit computational logical states $|00\rangle$, $|01\rangle$, $|10\rangle$, and $|11\rangle$ as well as the two qubit phase logical states $|++\rangle$, $|+-\rangle$, $| -+\rangle$, and $|--\rangle$.

At the end of the circuit we measure the qubits in the $|0, 1\rangle^{\otimes 8}$ basis for the computational logical states, or the $|+, -\rangle^{\otimes 8}$ basis for the phase logical states. As this is an error detecting code, if the measurement fails to satisfy the Z -checks, or X -checks of the $[[8, 2, 2]]$ code respectively, the result is discarded. Otherwise, an error is recorded when the measurement fails to lie within the X or Z -type stabilizer group of the $[[8, 2, 2]]$ code respectively.

Each of these circuits is run for 5000 shots. We also simulate these circuits for 50000 shots, with the error count then divided by 10. These results are tabulated in Table 1 with the logical fidelities calculated in Table 2. The (simulated) overall accept probability was $96 \pm 1\%$. From the experiments, it appears that the X basis is a more robust to noise than the Z , having no logical errors in SPAM or the CX experiments. We attribute the difference between the two basis to the difference circuit depth of the encoding circuits seen in Fig. 16. We note that these encoding circuits were not tested for fault-tolerant properties, meaning it was not confirmed that higher weight errors do not propagate through. Further analysis is needed to construct shallower, fault-tolerant encoding circuits and an general encoding protocol, but we leave this to future work.

6.3 The $[[10, 2, 3]]$ protocol

Here we benchmark the two qubit logical gate:

$$g = CX_{0,1} \cdot SWAP$$

	X basis	Z basis	Average
$SPAM_{exp}$	1.0000^{+0}_{-2}	0.9993^{+3}_{-3}	0.9996^{+2}_{-2}
$SPAM_{sim}$	0.9999^{+3}_{-3}	0.9988^{+1}_{-1}	0.9993^{+1}_{-1}
CX_{exp}	1.0000^{+0}_{-2}	0.9996^{+2}_{-2}	0.9998^{+1}_{-1}
CX_{sim}	0.99987^{+4}_{-4}	0.9991^{+1}_{-1}	0.9995^{+3}_{-3}

Table 2: The logical fidelities for state preparation and measurement (SPAM) as well as the CX implementation for the $[[8, 2, 2]]$ code. We note that X basis appears to perform better than Z basis, which we attribute to the depth of the encoding circuits used.

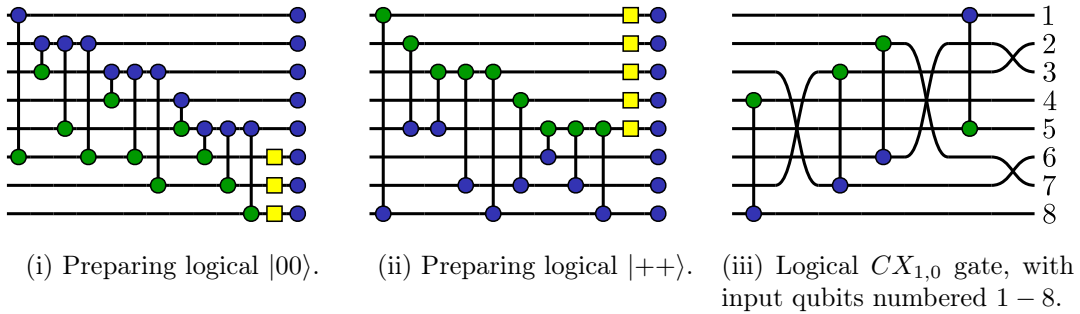


Figure 16: The $[[8,2,2]]$ Dehn twist protocol for benchmarking a logical CX gate. We note these encoding circuit have not been tested for fault-tolerant properties, and may lead to higher-weight physical errors to propagate to the logical state.

logical operation	logical state	experimental errors	simulated errors	logical operation	logical state	experimental errors	simulated errors
I	$ 00\rangle$	4	6.68	I	$ ++\rangle$	1	3.05
I	$ 11\rangle$	2	7.14	I	$ --\rangle$	3	3.16
g	$ 00\rangle$	6	14.18	g	$ ++\rangle$	8	12.30
g	$ 01\rangle$	7	13.84	g	$ +-\rangle$	2	12.65
g	$ 10\rangle$	4	14.29	g	$ -+\rangle$	3	12.58
g	$ 11\rangle$	2	14.97	g	$ --\rangle$	4	13.22

Table 3: The number of logical errors found for the $[[10, 2, 3]]$ code simulations and experiments. Here the logical operation I is meant to imply the state preparation and measurement errors seen while preparing the individual two-qubit logical states. A series of experiments were also performed implementing the logical g gate between the two logical qubits contained in the $[[10, 2, 3]]$ code block.

	X basis	Z basis	Average
$SPAM_{exp}$	0.9990^{+7}_{-7}	0.9985^{+8}_{-8}	0.9987^{+7}_{-7}
$SPAM_{sim}$	0.99844^{+8}_{-8}	0.9965^{+1}_{-1}	0.9974^{+1}_{-1}
g_{exp}	0.997^{+1}_{-1}	0.997^{+1}_{-1}	0.997^{+1}_{-1}
g_{sim}	0.9936^{+1}_{-1}	0.9928^{+1}_{-1}	0.9932^{+1}_{-1}

Table 4: The logical fidelities for state preparation and measurement (SPAM) as well as the g implementation. We note that X basis appears to perform better than Z basis, which we attribute to the depth of the encoding circuits used.

This is found as the lift of the order three (up to phase) transversal Clifford gate SH on the $[[5, 1, 3]]$ base code, using Theorem 3.7. See Fig. 17. We follow a similar benchmarking procedure as for the $[[8, 2, 2]]$ protocol above with 12 different circuits, except that instead of discarding measurements that present a non-zero syndrome we now infer a logical correction operator from the syndrome data using a *decoder algorithm*. This decoder accepts one of $2^4 = 16$ possible syndrome bits and outputs the most likely of the $2^2 = 4$ logical correction operators. We pre-calculate all of these using simulated data on 10^5 shots, and generate a lookup table. Note that we build a separate lookup table for each of the 16 circuits, in this way the decoder is aware of the specific noise model of that circuit. This improves the performance of the benchmark substantially. The shots where the decoder fails to give the correct logical operation are then recorded as errors.

We tabulate experimental results in Table 3 and fidelities of these operations in Table 4. Each circuit is run for 2000 shots. We also simulate each circuit for 2×10^5 shots and then normalize to 2000 shots. Similar to the $[[8, 2, 2]]$ results, we see a difference between the X basis and Z basis, with the X performing a bit better. We again attribute this to the circuit depth of the encoding circuits as seen in Fig. 17.

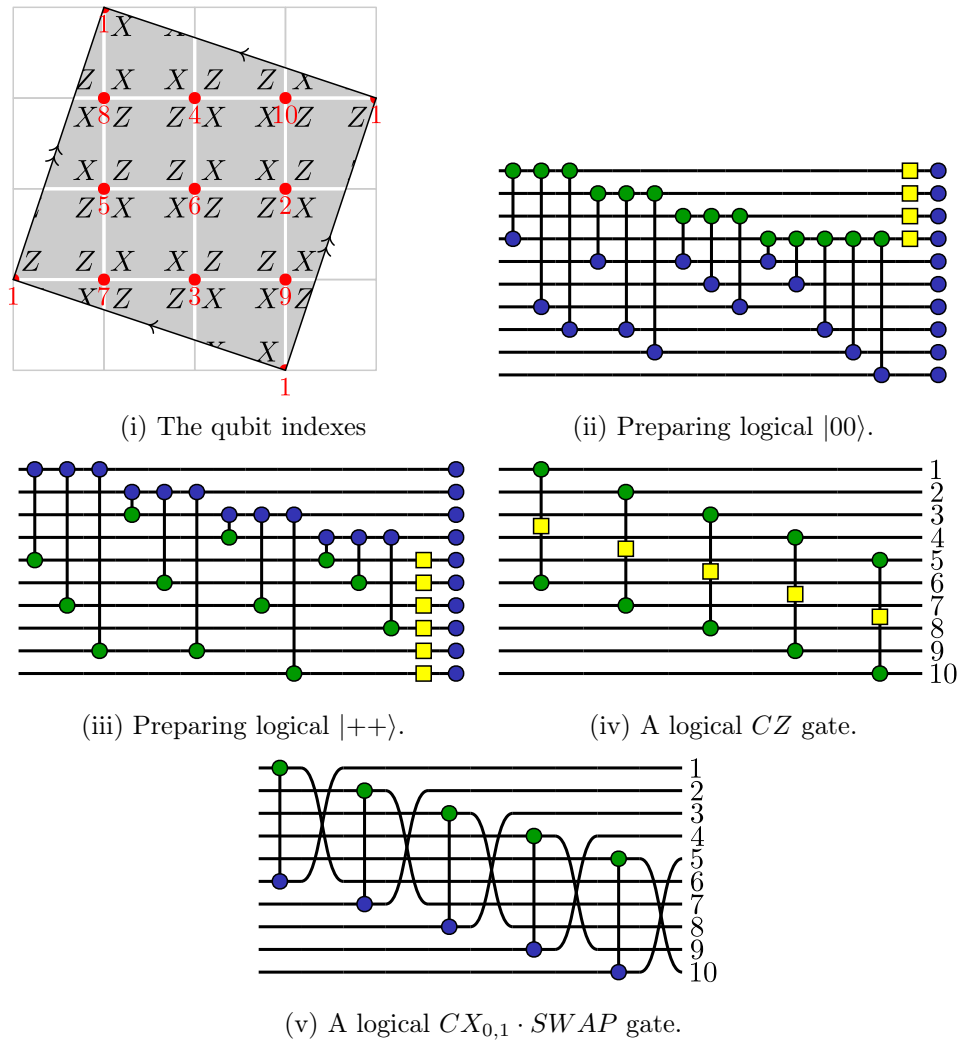


Figure 17: The $[[10,2,3]]$ protocol is derived from the $[[5,1,3]]$ base code.

7 Conclusion

As the field of quantum error correction advances, significant progress has been made in the design of quantum low-density parity check codes with favorable properties. However, many of these codes are limited by their scarcity of fault-tolerant logical operations. In this work we seek to *co-design* quantum codes that have both reasonable scaling properties as well as giving fault-tolerant logicals beyond the Pauli group.

Our study explores the use of covering spaces, a concept that underlies mathematical fields including Galois theory, number theory, and algebraic topology. Specifically, we focus on double covers within the realms of symplectic geometry, quantum codes, Riemann surfaces, and topological quantum codes. This multidisciplinary approach underscores a broader theoretical idea: two-dimensional topologically ordered systems should exhibit a correspondence between domain walls and covering spaces, particularly in the context of abelian domain walls.

A significant contribution of our work is the explicit protocol we develop for braiding genons and performing Dehn twists. This protocol leverages qubit permutations and constant depth Clifford circuits, which are efficiently realizable on quantum computers with high connectivity, such as Quantinuum’s H1-1. The practical implementation of these gates results in robust logical fidelity, showcasing the experimental viability of our approach.

Non-Clifford gates are essential for achieving universal fault-tolerant quantum computation. While Clifford gates alone form a useful set for many quantum operations, they are insufficient for universal quantum computing. Our construction lays the groundwork for integrating non-Clifford gates into the topological code framework, a critical step for universal fault-tolerant computation. Further research is required to fully develop and implement non-Clifford gates within these codes. Nonetheless, the methods and constructions found in this work appear promising and compatible with existing approaches, suggesting a viable pathway toward their realization.

Looking ahead, our findings suggest promising directions for further exploration. The correspondence between domain walls and covering spaces observed in two-dimensional topological systems could extend to three-dimensional systems. Such systems might exhibit defects whose statistics enable the generation of non-Clifford gates, pushing the boundaries of fault-tolerant quantum computation. Drawing inspiration from number theory, algebraic geometry, and related fields, we envision the development of more sophisticated quantum codes and fault-tolerant operations that could revolutionize quantum computing.

In conclusion, our work lays the groundwork for a unified theory that bridges diverse mathematical disciplines and advances the design of quantum error-correcting codes. By integrating twists, defects, and higher-dimensional topological structures, we open new pathways toward achieving versatile and scalable quantum computation with enhanced fault tolerance.

Acknowledgements. The authors thank Thomas Scruby, Michael Vasmer, Karl Mayer, Shival Dasu, Dan Gresh, and Pablo Andres-Martinez for useful conversations and feedback on this work.

References

- [1] M. Backens, S. Perdrix, and Q. Wang. A Simplified Stabilizer ZX-calculus. *Electronic Proceedings in Theoretical Computer Science*, 236:1–20, 2016.

- [2] C. Baldwin. Quantinuum hardware specifications. <https://github.com/CQCL/quantinuum-hardware-specifications>, 2022.
- [3] M. Barkeshli, P. Bonderson, M. Cheng, and Z. Wang. Symmetry fractionalization, defects, and gauging of topological phases. *Physical Review B*, 100(11):115147, 2019.
- [4] M. Barkeshli, C.-M. Jian, and X.-L. Qi. Twist defects and projective non-abelian braiding statistics. *Physical Review B*, 87(4):045130, 2013.
- [5] H. Bombín. Topological order with a twist: Ising anyons from an abelian model. *Physical review letters*, 105(3):030403, 2010.
- [6] H. Bombin, C. Dawson, R. V. Mishmash, N. Nickerson, F. Pastawski, and S. Roberts. Logical blocks for fault-tolerant topological quantum computation. *PRX Quantum*, 4(2):020303, 2023.
- [7] J. P. Bonilla Ataides, D. K. Tuckett, S. D. Bartlett, S. T. Flammia, and B. J. Brown. The XZZX surface code. *Nature communications*, 12(1):2172, 2021.
- [8] N. P. Breuckmann and S. Burton. Fold-Transversal Clifford Gates for Quantum Codes. *arXiv preprint arXiv:2202.06647*, 2022.
- [9] N. P. Breuckmann, C. Vuillot, E. Campbell, A. Krishna, and B. M. Terhal. Hyperbolic and semi-hyperbolic surface codes for quantum storage. *Quantum Science and Technology*, 2(3):035007, 2017.
- [10] B. J. Brown, K. Laubscher, M. S. Kesselring, and J. R. Wootton. Poking holes and cutting corners to achieve clifford gates with the surface code. *Physical Review X*, 7(2):021029, 2017.
- [11] A. R. Calderbank, E. M. Rains, P. M. Shor, and N. J. Sloane. Quantum error correction via codes over $gf(4)$. *IEEE Transactions on Information Theory*, 44(4):1369–1387, 1998.
- [12] N. Carqueville, M. Del Zotto, and I. Runkel. Topological defects. *arXiv preprint arXiv:2311.02449*, 2023.
- [13] B. Coecke and R. Duncan. Interacting quantum observables: categorical algebra and diagrammatics. *New Journal of Physics*, 13(4):043016, 2011.
- [14] J. Combes, C. Granade, C. Ferrie, and S. T. Flammia. Logical randomized benchmarking. *arXiv preprint arXiv:1702.03688*, 2017.
- [15] B. Criger and B. Terhal. Noise thresholds for the $[[4, 2, 2]]$ -concatenated toric code. *QIC*, 16(15-16):1261–1281, Nov 2016.
- [16] B. Farb and D. Margalit. *A primer on mapping class groups (pms-49)*, volume 41. Princeton university press, 2011.
- [17] E. Gironde and G. González-Diez. *Introduction to compact Riemann surfaces and dessins d'enfants*, volume 79. Cambridge University Press, 2012.
- [18] D. Gottesman. *Stabilizer codes and quantum error correction*. California Institute of Technology, 1997.

- [19] M. G. Gowda and P. K. Sarvepalli. Quantum computation with generalized dislocation codes. *Physical Review A*, 102(4):042616, 2020.
- [20] S. Gurevich and R. Hadani. The Weil representation in characteristic two. *Advances in Mathematics*, 230(3):894–926, 2012.
- [21] J. Haah. Algebraic methods for quantum codes on lattices. *Revista Colombiana de Matemáticas*, 50(2):295–345, 2016.
- [22] M. B. Hastings and A. Geller. Reduced space-time and time costs Ising dislocation codes and arbitrary ancillas. *Quantum Information and Computation*, 15(11-12):0962–0986, 2015.
- [23] M. Heinrich. *On stabiliser techniques and their application to simulation and certification of quantum devices*. PhD thesis, Universität zu Köln, 2021.
- [24] M. S. Kesselring, F. Pastawski, J. Eisert, and B. J. Brown. The boundaries and twist defects of the color code and their applications to topological quantum computation. *Quantum*, 2:101, 2018.
- [25] A. Kissinger. Phase-free ZX diagrams are CSS codes (... or how to graphically grok the surface code). *arXiv preprint arXiv:2204.14038*, 2022.
- [26] A. J. Landahl. The surface code on the rhombic dodecahedron. *arXiv preprint arXiv:2010.06628*, 2020.
- [27] A. Lavasani and M. Barkeshli. Low overhead clifford gates from joint measurements in surface, color, and hyperbolic codes. *Physical Review A*, 98(5):052319, 2018.
- [28] A. Lavasani, G. Zhu, and M. Barkeshli. Universal logical gates with constant overhead: instantaneous Dehn twists for hyperbolic quantum codes. *Quantum*, 3:180, Aug. 2019.
- [29] M. L. Liu, N. Tantivasadakarn, and V. V. Albert. Subsystem CSS codes, a tighter stabilizer-to-CSS mapping, and Goursat’s Lemma. *arXiv preprint arXiv:2311.18003*, 2023.
- [30] E. Magesan, J. M. Gambetta, and J. Emerson. Scalable and robust randomized benchmarking of quantum processes. *Phys. Rev. Lett.*, 106:180504, May 2011.
- [31] K. Mayer, C. Ryan-Anderson, N. Brown, E. Durso-Sabina, C. H. Baldwin, D. Hayes, J. M. Dreiling, C. Foltz, J. P. Gaebler, T. M. Gatterman, et al. Benchmarking logical three-qubit quantum fourier transform encoded in the steane code on a trapped-ion quantum computer. *arXiv preprint arXiv:2404.08616*, 2024.
- [32] J. Pino, J. Dreiling, and C. e. a. Figgatt. Demonstration of the trapped-ion quantum CCD computer architecture. <https://doi.org/10.1038/s41586-021-03318-4>, 2021.
- [33] R. Sarkar and T. J. Yoder. A graph-based formalism for surface codes and twists. *arXiv preprint arXiv:2101.09349*, 2021.
- [34] P. Selinger. Generators and relations for n-qubit clifford operators. *Logical Methods in Computer Science*, 11, 2015.

- [35] J. van de Wetering. Zx-calculus for the working quantum computer scientist. *arXiv preprint arXiv:2012.13966*, 2020.
- [36] D. J. Wineland, C. Monroe, W. M. Itano, D. Leibfried, B. E. King, and D. M. Meekhof. Experimental issues in coherent quantum-state manipulation of trapped atomic ions. *Journal of Research of the National Institute of Standards and Technology*, 103:259–328, May–June 1998.
- [37] T. J. Yoder and I. H. Kim. The surface code with a twist. *Quantum*, 1:2, 2017.
- [38] G. Zhu, A. Lavasani, and M. Barkeshli. Instantaneous braids and Dehn twists in topologically ordered states. *Physical Review B*, 102(7):075105, 2020.

A Fault-Tolerance of Fiber Transversal Gates

Given a base code with $m \times 2n$ check matrix $\mathcal{H} = (\mathcal{H}_X \ \mathcal{H}_Z)$, the doubled code $\mathfrak{D}(\mathcal{H})$ has a $2m \times 4n$ parity check matrix of the form 3, repeated here for convenient reference:

$$\mathfrak{D}(\mathcal{H}) := \begin{pmatrix} \mathcal{H}_X & \mathcal{H}_Z & 0 & 0 \\ 0 & 0 & \mathcal{H}_Z & \mathcal{H}_X \end{pmatrix}. \quad (5)$$

Theorem A.1. Given a fault-tolerant gate on quantum code C with parameters $[[n, k, d]]$, the lifted gate on the doubled code $\mathfrak{D}(C)$ is also fault-tolerant to at least distance d .

Proof. This proof will show a correspondence between the syndromes of faults on the base and lifted codes. If the gate on the base code tolerates the original fault up to weight $t = \lfloor \frac{d-1}{2} \rfloor$, the lifted gate on the doubled code tolerates the transformed fault.

If a gate on the base code is supported on qubit i on the base code, in the doubled code, the lifted gate has a two-qubit gate supported on qubits i and $i + n$.

Given a fault $f \in \mathbb{F}_2^n \oplus \mathbb{F}_2^n$ written in block column form:

$$f = \begin{pmatrix} f_X \\ f_Z \end{pmatrix}, \quad (6)$$

we define the *syndrome* of the fault, $S_f \in \mathbb{F}_2^m$:

$$S_f := \mathcal{H}\Omega_n f = (\mathcal{H}_X \ \mathcal{H}_Z)\Omega_n \begin{pmatrix} f_X \\ f_Z \end{pmatrix} = \mathcal{H}_X f_Z + \mathcal{H}_Z f_X. \quad (7)$$

For the remainder of the proof, we will speak about some single, constant fault f .

In the doubled code, the syndrome of a fault $f' \in \mathbb{F}_2^{2n} \oplus \mathbb{F}_2^{2n}$ is $\mathbf{S}_{f'} \in \mathbb{F}_2^{2m}$.

$$\mathbf{S}_{f'} = \begin{pmatrix} \mathcal{H}_X & \mathcal{H}_Z & 0 & 0 \\ 0 & 0 & \mathcal{H}_Z & \mathcal{H}_X \end{pmatrix} \Omega_{2n} \begin{pmatrix} f'_X \\ f'_Z \end{pmatrix} = (\mathcal{H}_X \mathcal{H}_Z) f'_Z \oplus (\mathcal{H}_Z \mathcal{H}_X) f'_X. \quad (8)$$

Since the doubled code is a CSS code, we may break the syndrome into X and Z components. The doubled parity check matrix also has equal size X and Z components, so the syndrome may be represented:

$$\mathbf{S}_{f'} = \mathbf{S}_{f'}^X \oplus \mathbf{S}_{f'}^Z \quad \mathbf{S}_{f'}^X, \mathbf{S}_{f'}^Z \in \mathbb{F}_2^m. \quad (9)$$

These parts of the syndromes are calculated:

$$\mathbf{S}_{f'}^X = (\mathcal{H}_X \mathcal{H}_Z) f'_Z \quad \mathbf{S}_{f'}^Z = (\mathcal{H}_Z \mathcal{H}_X) f'_X. \quad (10)$$

We observe that, using 10 and 7, if $f'_Z = \begin{pmatrix} f_Z \\ f_X \end{pmatrix}$, then $\mathbf{S}_{f'}^X = S_f$. Note that $w \begin{pmatrix} f_Z \\ f_X \end{pmatrix} = w \begin{pmatrix} f_X \\ f_Z \end{pmatrix}$. Therefore, if there is a decoder on the base such that it corrects all $\{f | w(f) \leq t\}$, there is also a decoder on the lifted code which corrects all f'_Z of the form $\begin{pmatrix} f_Z \\ f_X \end{pmatrix}$.

In particular, a t -fault-tolerant base code corrects Y -type Pauli faults of weight less than t . Y -type errors of this form satisfy $f_Z = f_X$ and $w(f) = w(f_Z) = w(f_X) \leq t$. For clarity, we will represent these symmetric faults as $\begin{pmatrix} f_Y \\ f_Y \end{pmatrix}$. This implies that the doubled code can correct faults of the form $\begin{pmatrix} f_Y \\ f_Y \end{pmatrix}$ where $w(f_Y) \leq t$, or in Pauli notation $Z_i Z_{i+n}$. These are exactly the weight two Z -type faults resulting from lifted gates on the doubled code. Also, a t -fault-tolerant base code can correct X and Z type faults with block forms $\begin{pmatrix} f_X \\ 0 \end{pmatrix}$ and $\begin{pmatrix} 0 \\ f_Z \end{pmatrix}$ respectively. Thus, the doubled code can correct all faults of the form $\begin{pmatrix} f_Y + f_X \\ f_Y + f_Z \end{pmatrix}$ satisfying $w(f_X) + w(f_Y) + w(f_Z) \leq t$, which spans the space of up to t faults on lifted gates.

Since the doubled code is a CSS code, the proof for X -type faults is the same, but with the roles of \mathcal{H}_X and \mathcal{H}_Z reversed. □

B Example QASM

This is QASM source for an example of the $[[4, 1, 2]]$ randomized benchmarking protocol of length $N = 2$. We show the qubit permutations as $P(\dots)$ operations as well as the resulting labels in comments.

```
OPENQASM 2.0;
include "hqslib1.inc";

qreg q[4];
creg m[4];

reset q;

// prepare logical |0> state
h q[1]; h q[0]; cy q[0], q[1]; h q[2];
cy q[1], q[2]; cx q[0], q[3]; h q[0]; x q[0]; z q[0];
barrier q;
```

```

// First logical Clifford
x q[2]; x q[0];
// P(0, 2, 1, 3)
// labels = [0, 2, 1, 3]
s q[3]; s q[1]; h q[1]; h q[2]; s q[2]; s q[0]; h q[0]; s q[0];
// P(0, 3, 2, 1)
// labels = [0, 3, 1, 2]
x q[1]; x q[0]; h q[2]; h q[1]; h q[3]; h q[0]; x q[1]; z q[3]; x q[1]; x q[0];
// P(0, 2, 1, 3)
// labels = [0, 1, 3, 2]
s q[2]; s q[3]; h q[3]; h q[1]; s q[1]; s q[0]; h q[0]; s q[0];
// P(0, 3, 2, 1)
// labels = [0, 2, 3, 1]
x q[3]; x q[0]; h q[1]; h q[3]; h q[2]; h q[0]; x q[3]; z q[2]; x q[2]; z q[0];
barrier q;

// Second logical Clifford
x q[3]; x q[0];
// P(0, 2, 1, 3)
// labels = [0, 3, 2, 1]
s q[1]; s q[2]; h q[2]; h q[3]; s q[3]; s q[0]; h q[0]; s q[0];
// P(0, 3, 2, 1)
// labels = [0, 1, 2, 3]
x q[2]; x q[0]; h q[3]; h q[2]; h q[1];
h q[0]; x q[2]; z q[1]; x q[2]; z q[1]; x q[1]; z q[0];
barrier q;

// decode
cy q[0], q[1]; cz q[0], q[2]; h q[0];
cy q[1], q[2]; cz q[1], q[3]; h q[1];
cz q[2], q[0]; cy q[2], q[3]; h q[2];
sdg q[3]; h q[3]; s q[3];

// inverse of logical Clifford
x q[3]; z q[3]; h q[3]; sdg q[3];
x q[3]; h q[3]; sdg q[3]; h q[3];
sdg q[3];

measure q -> m;
// final qubit order: [0, 1, 2, 3]

```

For the $[[8, 2, 2]]$ protocol, we show example QASM preparing the $|0, 1\rangle$ state and applying the fault-tolerant Clifford gate $CX_{0,1} \cdot SWAP$.

```

OPENQASM 2.0;
include "hqslib1.inc";

```



```

qreg q[8];
creg m[8];

reset q;

h q[7]; h q[6]; h q[5];
cx q[7], q[4]; cx q[6], q[4]; cx q[5], q[4];
cx q[4], q[3]; cx q[6], q[2]; cx q[5], q[2];
cx q[3], q[2]; cx q[5], q[1]; cx q[4], q[1];
cx q[2], q[1]; cx q[5], q[0];
x q[4]; x q[1];
barrier q;

// P(0, 2, 1, 3, 4, 6, 5, 7)
// labels = [0, 2, 1, 3, 4, 6, 5, 7]
cx q[4], q[0];
// P(0, 5, 2, 3, 4, 1, 6, 7)
// labels = [0, 6, 1, 3, 4, 2, 5, 7]
cx q[6], q[2];
cx q[1], q[5];
// P(0, 1, 6, 3, 4, 5, 2, 7)
// labels = [0, 6, 5, 3, 4, 2, 1, 7]
cx q[3], q[7];
barrier q;

x q[4]; x q[6]; x q[7]; x q[0];
measure q -> m;

// final qubit order: [0, 6, 5, 3, 4, 2, 1, 7]

```

Here is a circuit for the $[[10,2,3]]$ protocol, acting on logical $|+-\rangle$:

```

OPENQASM 2.0;
include "hqslib1.inc";

qreg q[10];
creg m[10];

reset q;

h q[9]; h q[8]; h q[7]; h q[6]; h q[5]; h q[4];
cx q[7], q[3]; cx q[5], q[3]; cx q[4], q[3];
cx q[9], q[2]; cx q[6], q[2]; cx q[3], q[2];
cx q[8], q[1]; cx q[5], q[1]; cx q[2], q[1];
cx q[8], q[0]; cx q[6], q[0]; cx q[4], q[0];
barrier q;

```

```

z q[5]; z q[4]; z q[1];
barrier q;

// P(0, 1, 2, 3, 9, 5, 6, 7, 8, 4)
// labels = [0, 1, 2, 3, 9, 5, 6, 7, 8, 4]
cx q[9], q[4];
// P(0, 1, 2, 8, 4, 5, 6, 7, 3, 9)
// labels = [0, 1, 2, 8, 9, 5, 6, 7, 3, 4]
cx q[8], q[3];
// P(0, 1, 7, 3, 4, 5, 6, 2, 8, 9)
// labels = [0, 1, 7, 8, 9, 5, 6, 2, 3, 4]
cx q[7], q[2];
// P(0, 6, 2, 3, 4, 5, 1, 7, 8, 9)
// labels = [0, 6, 7, 8, 9, 5, 1, 2, 3, 4]
cx q[6], q[1];
// P(5, 1, 2, 3, 4, 0, 6, 7, 8, 9)
// labels = [5, 6, 7, 8, 9, 0, 1, 2, 3, 4]
cx q[5], q[0];
barrier q;

z q[9]; z q[8]; z q[7]; z q[6]; z q[5];
barrier q;

h q[4]; h q[3]; h q[2]; h q[1]; h q[0];
h q[9]; h q[8]; h q[7]; h q[6]; h q[5];
measure q -> m;

// final qubit order: [5, 6, 7, 8, 9, 0, 1, 2, 3, 4]

```